Integrating Concentrating Solar Power Technologies into the Hybrid Optimization and Performance Platform (HOPP)

William Hamilton,[1] Janna Martinek,[1] John Cox,[2] and Alexandra Newman[2]

1 National Renewable Energy Laboratory
2 Colorado School of Mines

NREL is a national laboratory of the U.S. Department of Energy
Office of Energy Efficiency & Renewable Energy
Operated by the Alliance for Sustainable Energy, LLC

This report is available at no cost from the National Renewable Energy Laboratory (NREL) at www.nrel.gov/publications.

Contract No. DE-AC36-08GO28308

Technical Report
NREL/TP-5700-82726
August 2022

Integrating Concentrating Solar Power Technologies into the Hybrid Optimization and Performance Platform (HOPP)

William Hamilton,[1] Janna Martinek,[1] John Cox,[2] and Alexandra Newman[2]

1 National Renewable Energy Laboratory
2 Colorado School of Mines

Suggested Citation
Hamilton, William, Janna Martinek, John Cox, and Alexandra Newman. 2022. *Integrating Concentrating Solar Power Technologies into the Hybrid Optimization and Performance Platform (HOPP)*. Golden, CO: National Renewable Energy Laboratory. NREL/TP-5700-82726. https://www.nrel.gov/docs/fy22osti/82726.pdf.

NREL is a national laboratory of the U.S. Department of Energy
Office of Energy Efficiency & Renewable Energy
Operated by the Alliance for Sustainable Energy, LLC

This report is available at no cost from the National Renewable Energy Laboratory (NREL) at www.nrel.gov/publications.

Contract No. DE-AC36-08GO28308

Technical Report
NREL/TP-5700-82726
August 2022

National Renewable Energy Laboratory
15013 Denver West Parkway
Golden, CO 80401
303-275-3000 • www.nrel.gov

NOTICE

This work was authored in part by the National Renewable Energy Laboratory, operated by Alliance for Sustainable Energy, LLC, for the U.S. Department of Energy (DOE) under Contract No. DE-EE00034455. Funding provided by the U.S. Department of Energy Office of Energy Efficiency and Renewable Energy Solar Energy Technologies Office. Additionally, this work was in part funded by The World Bank Group in collaboration with Solar Dynamics LLC under Contract No. 7201329. The views expressed herein do not necessarily represent the views of the DOE or the U.S. Government.

Cover Photos by Dennis Schroeder: (clockwise, left to right) NREL 51934, NREL 45897, NREL 42160, NREL 45891, NREL 48097, NREL 46526.

Executive Summary

As the world increases renewable energy deployment, there is a growing interest in hybridizing various generation and storage technologies to maximize net benefit to the developer and/or off-taker. A particularly interesting combination of renewable technologies is concentrating solar power (CSP) with thermal energy storage (TES), photovoltaics (PV), and electrochemical battery energy storage systems (BESS). The hybridization of CSP with TES, PV, and BESS has the potential to provide continuous high-capacity factor energy production at a lower cost than a PV-BESS or CSP system alone. This configuration could service either a grid connection or a remote load that requires minimal variability in its generation profile, e.g., mining operations.

Because of the system complexity of CSP technology, it is difficult to evaluate the technological and financial performance of a CSP-PV hybrid system without detailed modeling of annual operations. To address this challenge, we have developed a modeling framework for evaluating the performance and financial viability of CSP systems hybridized with PV and battery technologies. This modeling effort incorporates CSP tower and trough systems into an existing modeling tool recently developed by NREL, the Hybrid Optimization and Performance Platform (HOPP) (Tripp et al. 2019).

This report outlines the modeling methodology as well as preliminary results from example case studies conducted using the model. The methodology describes: (i) the integration of CSP power tower and parabolic trough into HOPP using Python interfaces to access System Advisor Model (SAM) underlying technology models, (ii) the mathematical formulation of the mixed integer linear program dispatch optimization model, which optimizes operations of storage assets to either maximize system revenue or minimize operating cost while load following, (iii) the design analysis methods implemented within HOPP, and (iv) simulation clustering for the purpose of reducing computational expense. We exercise the model using a case study of a future scenario where we assume (i) CSP and PV technologies achieve the 2030 cost targets provided by the Solar Energy Technologies Office (SETO), (ii) battery costs reduce to the 2030 mid-cost projection presented by NREL (Cole, Frazier, and Augustine 2021), (iii) electricity prices for southern California in 2030 are provided by NREL's Cambium database (Gagnon et al. 2020), and (iv) a capacity payment of $150/kW-yr based on the system capacity factor during the top 100 net-load hours (Jorgenson, Denholm, and Mehos 2014).

Within this report, we determine that CSP with TES hybridized with PV provides the best benefit-to-cost ratio compared to the other simulated technology combinations. However, this configuration only increases the benefit-to-cost ratio by about 1% compared to the CSP with TES configuration. The PV-battery system provides the lowest benefit-to-cost ratio compared to the other configurations explored because of the low capacity credit received by the system. This low capacity credit was due to the trade-off between the cost of increasing battery energy capacity and additional revenue provided to the system by increasing the capacity credit. Additionally, we present the difference in benefit-to-cost ratio determined by running a full annual simulation and representative day clustering. For our case study, the best design selected using the representative day clustering was at worst 2% lower in benefit-to-cost ratio than the best design selected using the full annual simulations.

Our approach provides a methodology for modeling CSP with TES hybridized with PV as well as hybrid PV-battery systems enabling a direct comparison of the technology configurations. This modeling framework is based on hourly time fidelity, which can provide insight about how bulk energy generation can be shifted to high-value and/or high-load hours; however, the model is currently incapable of capturing fine time-fidelity behavior that could be very valuable in balancing generation. Specifically, in a configuration that includes CSP with TES hybridized with PV and batteries, the battery could provide frequency response and a "buffer" between transitions of CSP and PV generation which could be very valuable if the system was powering a remote load without a grid interconnect.

Acknowledgments

This work was authored in part by the National Renewable Energy Laboratory, operated by Alliance for Sustainable Energy, LLC, for the U.S. Department of Energy (DOE) under Contract No. DE-EE00034455 titled "Valuation and Operational Performance of Solar plus Storage Power Plants." Funding provided by the U.S. Department of Energy Office of Energy Efficiency and Renewable Energy Solar Energy Technologies Office. The views expressed in the article do not necessarily represent the views of the DOE or the U.S. Government. The U.S. Government retains and the publisher, by accepting the article for publication, acknowledges that the U.S. Government retains a nonexclusive, paid-up, irrevocable, worldwide license to publish or reproduce the published form of this work, or allow others to do so, for U.S. Government purposes. Additionally, this work was in part funded by The World Bank Group in collaboration with Solar Dynamics LLC under Contract No. 7201329 titled "Modeling Dispatchable Hybrid Solar Power and Energy Storage Systems in Tunisia."

The authors of this report would like to acknowledge the contributions of Matt Boyd at NREL for his work on the implementation of capacity credit calculations within HOPP and his work with the parabolic trough CSP model within SSC.

List of Acronyms

API Application programming interface

BA Balancing area

BESS Battery energy storage systems

CAISO California Independent System Operator

CSP Concentrating solar power

DNI Direct normal irradiance

DOE Department of Energy

GHI Global horizontal irradiance

HOPP Hybrid Optimization and Performance Platform

HTF Heat transfer fluid

IRENA International Renewable Energy Agency

LCOE Levelized cost of energy

LMP Locational marginal price

MILP Mixed integer linear program

NREL National Renewable Energy Laboratory

RMS Root-mean-square

SAM System Advisor Model

SETO Solar Energy Technologies Office

SOC State of charge

SSC SAM Simulation Core

PPA Power purchase agreement

PV Photovoltaics

TES Thermal energy storage

TMY Typical meteorological year

Table of Contents

Executive Summary . . . iv
Acknowledgments . . . v
List of Acronyms . . . vi
1 Introduction . . . 1
2 Methodology . . . 3
2.1 Integration of CSP into HOPP . . . 5
2.1.1 Annual Performance Simulation . . . 5
2.1.2 Parameter Scaling . . . 6
2.1.3 Capacity Value . . . 7
2.2 Dispatch Optimization . . . 8
2.2.1 Mathematical Formulation . . . 9
2.2.2 Operational Costs . . . 17
2.2.3 Example Dispatch Profiles . . . 17
2.3 Design Analysis . . . 21
2.3.1 Problem Driver Class . . . 21
2.3.2 Hybrid Sizing Problem . . . 22
2.3.3 Design Sampling . . . 22
2.3.4 Design Optimization . . . 22
2.4 Simulation Clustering . . . 23
2.4.1 Weighting Factors . . . 23
3 Case Studies . . . 26
3.1 Example Future Scenario . . . 26
3.1.1 Input Data . . . 26
3.1.2 Analysis Methods . . . 28
3.1.3 Results . . . 29
3.2 Design Space Sampling Using Representative Days . . . 32
4 Summary, Conclusions, and Future Work . . . 35
References . . . 38

List of Figures

Figure 1. A CSP tower configuration hybridized with photovoltaics and batteries. . . . 3

Figure 2. A parabolic trough oil CSP configuration with indirect molten salt storage hybridized with photovoltaics and batteries. . . . 3

Figure 3. Overview of the HOPP software framework: price-taker dispatch optimization governs time-dependent subsystem operations, and nonlinear optimization algorithms are used to determine the optimal value of high-level design and sizing variables. . . . 4

Figure 4. Information flow for design performance evaluation for a hybrid system involving CSP and battery technologies, specifically focusing on tower CSP configuration. . . . 6

Figure 5. HOPP hybrid simulation dispatch optimization module approach. . . . 9

Figure 6. Example simulated dispatch profile for a PV + Battery system with a 200 MW_e (DC) PV array, DC-to-AC ratio of 1.5, 100 MW_e / 400 MWh_e battery, and a grid limit of 100 MW_e. . . . 18

Figure 7. Example simulated dispatch profile for a CSP + TES system with a 100 MW_e (gross) power cycle, solar multiple of 2.5, 15 hours of thermal storage, and a grid limit of 100 MW_e. 19

Figure 8. Example simulated dispatch profile for a CSP + TES + PV system with a 100 MW_e (gross) power cycle, solar multiple of 2.0, 15 hours of thermal storage, 100 MW_e (DC) PV array, DC-to-AC ratio of 1.5, and a grid limit of 100 MW_e. 19

Figure 9. Example simulated dispatch profile for a CSP + TES + PV + Battery system with a 75 MW_e (gross) power cycle, solar multiple of 2.0, 15 hours of thermal storage, 100 MW_e (DC) PV array, DC-to-AC ratio of 1.5, 25 MW_e / 100 MWh_e battery, and a grid limit of 100 MW_e. 20

Figure 10. Simple depiction of the problem driver class facilitating design analysis through HOPP's design analysis methods and interacting with the worker pool. 21

Figure 11. RMS fractional error in annual revenue over all scenarios in Table 8 with $N^c = 20$ and $N^c = 30$. Weighting sets are sorted from best-to-worst based on RMS error over all simulated design configurations for each (a) CSP + TES, (b) CSP + TES + PV + Battery. 24

Figure 12. Fractional error in annual revenue for CSP + TES + PV + Battery cases for individual weather-price scenarios (RMS over $N^c = 20, 30$). Weighting sets are identical to those in Figure 11(b) but are sorted from low-to-higher error for each location. 25

Figure 13. Daily price distributions from the Cambium 2020 mid-case scenario for model year 2030 and balancing area 10 (southern California). 27

Figure 14. Benefit-to-cost ratios as a function of the design variables with the "best" regions highlighted. . . 29

Figure 15. Capacity credit of the PV battery configuration for all the samples explored as a function of PV capacity, DC-to-AC ratio, and battery capacity. 31

Figure 16. System benefit-to-cost ratio (relative to the best simulated design) without capacity value for 200 randomly-sampled sets of design parameters using full simulations and simulations based on 10, 20, or 30 clusters. Sets of design parameters are sorted from highest-to-lowest benefit-to-cost ratio using full simulation results. 32

Figure 17. System benefit-to-cost ratio (relative to the best simulated design) including \$150/kW-yr capacity payment for 200 randomly-sampled sets of design parameters using full simulations and simulations based on 10, 20, or 30 clusters. Sets of design parameters are sorted from highest-to-lowest benefit-to-cost ratio using full simulation results. 33

Figure 18. Objective functions (relative to the best simulated design) for 200 randomly-sampled sets of design parameters for a hybrid CSP+TES+PV+Battery system using full simulations and simulations based on 10, 20, or 30 clusters. Sets of design parameters are sorted from best to worst objective using full simulation results. 34

List of Tables

Table 1. Parameters for the CSP technology dispatch module. 10

Table 2. Variables for the CSP technology dispatch module. 11

Table 3. PV dispatch module parameters and variables. 13

Table 4. Battery dispatch module parameters and variables. 14

Table 5. Electric grid dispatch module parameters and variables. 15

Table 6. Hybrid dispatch module parameters. 15

Table 7. Hybrid dispatch cost coefficient default values. †The parameter value is scaled based on subsystem capacity. 17

Table 8. Location, weather, and pricing scenarios used to select weighting factors for clustering. Price signals from NREL's Cambium are from the balancing area (BA) consistent with the location of the scenario. 24

Table 9. SAM's PVWatts installation cost parameters used to estimate HOPP's cost per DC capacity. All other inputs on the *Installation Costs* page were assumed to be zero. Assumed O&M costs are also included in this table. 26

Table 10. SAM molten-salt power tower single-owner installation cost parameters used to represent the SETO 2030 cost targets. All other inputs included on the *Installation Costs* page were assumed to be zero. Assumed O&M costs are also included in this table. 27

Table 11. System sizing design variables and associated ranges for each technology. †Cycle capacity and battery rating were varied only for the CSP with TES co-located with PV with battery storage case, and the sum of the two capacity variables was required to equal the 100 MWe "dispatchable" power rating. . . 28

Table 12. Performance and financial metrics corresponding to the maximum benefit-to-cost ratio found for each configuration. Note the red and green text indicate the worst and best values for that metric across the set of simulated technology combinations, respectively. 30

Table 13. Design variable values corresponding to the maximum benefit-to-cost ratio found for each configuration. Note the red text indicates the values that were constrained in this analysis. †Values correspond with variable bound. 31

Table 14. Difference in benefit/cost ratio for the best design identified using simulations based on 10, 20, or 30 clusters, relative to the best design identified from full simulations out of 200 randomly-sampled sets of design parameters 34

1 Introduction

As the world increases renewable energy deployment, there is a growing interest in hybridizing various generation and storage technologies to maximize net benefit to the developer and/or off-taker. A particularly interesting combination of renewable technologies is concentrating solar power (CSP) with thermal energy storage (TES), photovoltaics (PV), and electrochemical battery energy storage systems (BESS). The hybridization of CSP with TES, PV, and BESS has the potential to provide continuous high-capacity factor energy production at a lower cost than a PV-BESS or CSP system alone. This configuration could service either a grid connection or a remote load that requires minimal variability in its generation profile, e.g., mining operations.

Unlike PV technology, which converts sunlight directly to electricity, CSP systems use arrays of mirrors to reflect and concentrate solar energy onto a solar receiver. A heat transfer fluid (HTF) within the receiver absorbs the solar energy, and the high-temperature HTF can be stored in insulated storage tanks and dispatched as needed to a thermodynamic power cycle to produce electricity. Both CSP and PV technologies use incoming solar irradiation as their energy resource; however, CSP uses only direct normal irradiance (DNI) while PV uses global horizontal irradiance (GHI), which is the combination of DNI and diffuse irradiance. As a result, locations that are favorable for CSP deployment, i.e., places with a high DNI resource, will inherently be favorable for PV deployment. Therefore, CSP must be designed to interact seamlessly with PV in future electricity grids.

In the last decade, the cost of PV systems has decreased significantly. According to the International Renewable Energy Agency (IRENA), the levelized cost of energy (LCOE) of utility-scale PV systems decreased by 85% between 2010 and 2020, from $381/MWh to $57/MWh in 2020 (IRENA 2021). CSP costs have also decreased over the last decade, but at a slower rate than PV systems. The LCOE of CSP systems decreased by 68% between 2010 and 2020, from $340/MWh to $108/MWh in 2020 (IRENA 2021). However, less than a handful of CSP plants were commissioned in 2020, which dwarfs in comparison to the number of PV plants commissioned in 2020. Cost targets established by the U.S. Department of Energy (DOE) set a $0.05/kWh target for a dispatchable high-capacity factor CSP system with storage by 2030, and $0.03/kWh, $0.04/kWh, and $0.05/kWh targets for utility-scale, commercial, and residential PV systems by 2030, respectively (Solar Energy Technologies Office). Analysis has indicated that the role of CSP in the capacity and electricity generation mix within the U.S. electric grid is expected to expand only if these 2030 cost targets are realized (Murphy et al. 2019).

Given these cost trends and the co-location of solar resource, it is difficult for CSP technologies to directly compete with PV generation during the solar day. However, CSP can readily pair with low-cost TES, which enables electricity generation outside of the solar day or during cloudy periods. While PV system costs are low, storing bulk energy (greater than 2 to 4 hours of capacity) through lithium-ion batteries is not cost competitive (Shan et al. 2022; Hunter et al. 2021). Therefore, hybridizing CSP and PV technologies could provide a cost-effective system to provide high capacity factor electricity generation.

As a result, there has been increasing interest in hybridization of CSP and PV technologies in the CSP industry and the CSP research community (Kong et al. 2022; Liu et al. 2022; Hamilton et al. 2020; Parrado et al. 2016; Cocco, Migliari, and Petrollese 2016; Green et al. 2015). However, given the system complexity of CSP technology, it is difficult to evaluate the technological and financial performance of a CSP-PV hybrid system without detailed modeling of annual operations. To address this challenge, we have developed a modeling framework for evaluating the performance and financial viability of CSP systems hybridized with PV and battery technologies. This modeling effort incorporates CSP tower and trough systems into an existing modeling tool recently developed by NREL, the Hybrid Optimization and Performance Platform (HOPP) (Tripp et al. 2019).

HOPP is a Python-based modeling tool to evaluate the performance and financial viability of hybrid renewable energy systems. Hybrid power systems can be broadly defined as systems involving multiple energy generation, storage, and/or conversion technologies that are integrated—through an overarching control framework or physically—to achieve cost savings and enhanced capabilities, value, efficiency, or environmental performance compared to the independent alternatives (U.S. Department of Energy (DOE) 2021). HOPP was originally developed to evaluate PV-wind-battery hybrid systems; however, HOPP was built to allow other technologies to be included in future development. In this work, we developed capabilities to evaluate CSP systems within the HOPP framework—specifically, commercially-deployed power tower and parabolic trough CSP configurations with molten salt TES.

This report outlines the modeling methodology as well as preliminary results from example case studies conducted using the model. Section 2 describes the methodology of incorporating CSP into HOPP, the development of the dispatch optimization model within HOPP, the integration of data clustering techniques to reduce annual simulation times, and the development of design analysis methods to iterate on key design variables to minimize or maximize a user-defined objective function. Section 3 describes an example case study examining sensitivity of financial performance to design configurations based on a projected future grid and technology cost scenario. Section 4 summarizes this work with conclusions and future work.

2 Methodology

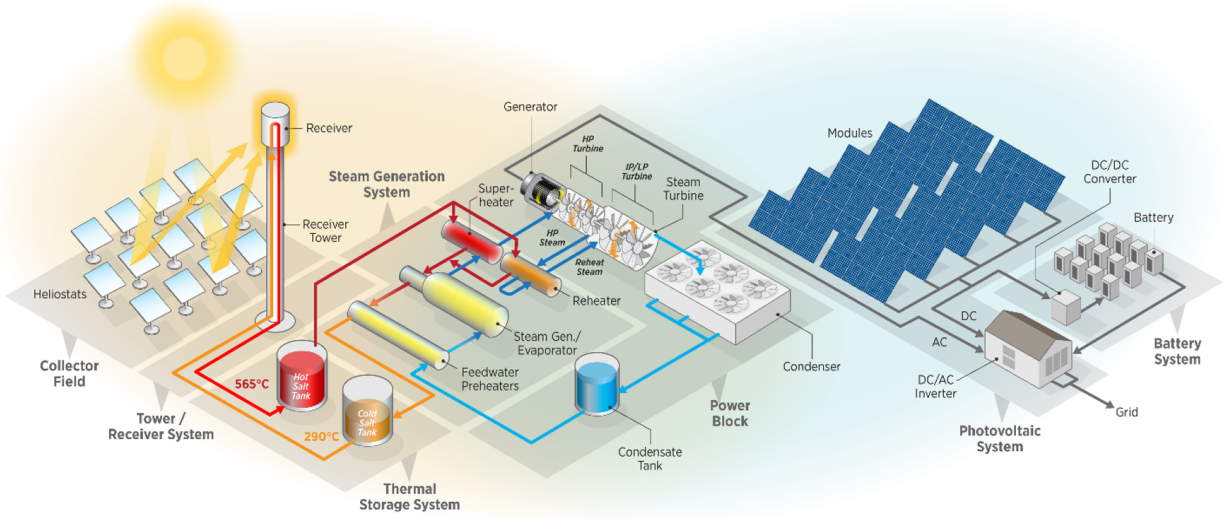

Figure 1. A CSP tower configuration hybridized with photovoltaics and batteries.

This section presents our methodology for integrating power tower and parabolic trough CSP configurations into HOPP. Figure 1 depicts a molten-salt tower CSP configuration hybridized with photovoltaics and batteries. In this configuration, the CSP and PV systems are co-located and are assumed to operate behind the same grid interconnect. The PV system power can be dispatched to the grid, stored in the battery system, used to supply CSP parasitic power requirements, or curtailed. The molten-salt tower CSP configuration uses a field of solar tracking mirrors, called heliostats, to concentrate the solar irradiance to a central receiver. Molten salt flows within the receiver and is heated from about 290°C to about 565°C. The molten salt is stored in tanks until electricity generation is desired, where the salt then flows through a series of salt-to-steam heat exchangers to generate superheated steam which drives a traditional Rankine steam cycle.

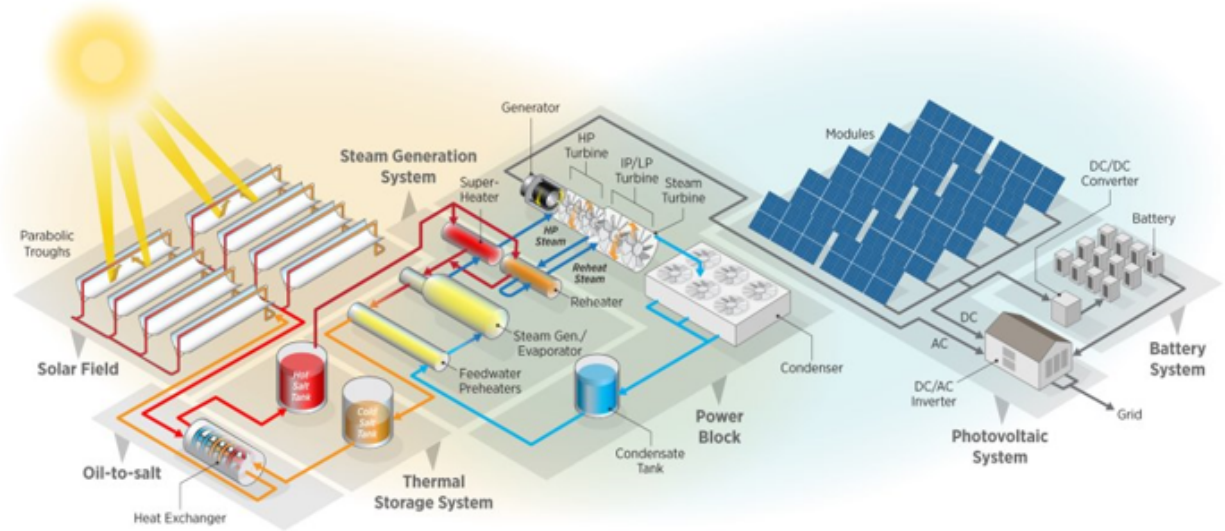

Figure 2. A parabolic trough oil CSP configuration with indirect molten salt storage hybridized with photovoltaics and batteries.

Figure 2 depicts a parabolic trough oil CSP configuration with indirect molten salt storage hybridized with photovoltaics and batteries. This configuration is identical to the tower configuration except for the solar collection field. In the parabolic trough configuration, thermal oil is pumped through the solar field and is heated from about 290°C to about 390°C. Once heated, the oil passes through an oil-to-salt heat exchanger where the heat is transferred to molten salt for storage until electricity generation is desired. There is ongoing research in heating molten salt directly

using the solar collection field; however, this system has not been built on a commercial scale at the time of writing of this report. The thermal oil used in parabolic trough CSP systems limits the maximum temperature within the system to about 390°C, which results in lower Rankine cycle thermal efficiency.

Further hybridization of CSP and PV technologies could occur by introducing an electric heater within the molten salt storage loop (within both tower and trough configurations), which would enable the molten salts to store any curtailed PV generation that the battery is unable to store. Additionally, this electric heater could be used for grid energy arbitrage similar to electrochemical batteries. Other suggested hybrid configurations utilize electricity generated by PV and an electric heater to boost the temperature of the HTF leaving the CSP receiver, thereby producing a higher power cycle efficiency. These configurations more intricately link the CSP and PV systems and were not considered in this effort, but adding this modeling capability is of interest in future work.

Figure 3 depicts an overview of the HOPP software framework. From the HOPP Python interface, users can provide (i) locational weather data for a specific project site of interest in the form of a typical meteorological year (TMY) or single-year weather file, (ii) market conditions in the form of assumed grid prices available to plant, and (iii) any technology-specific performance, cost, or financial parameter assumptions. The Python user interface is flexible to enable custom modeling efforts. HOPP can be used to evaluate annual techno-economic metrics for a single hybrid design under specific assumptions. For any given hybrid system design, HOPP uses a price-taker dispatch optimization model to optimize operations over a given horizon to either maximize plant revenue or minimize operating cost while following a user-provided load signal. Additionally, HOPP can be used to iterate on high-level design variables to minimize or maximize a specific design objective.

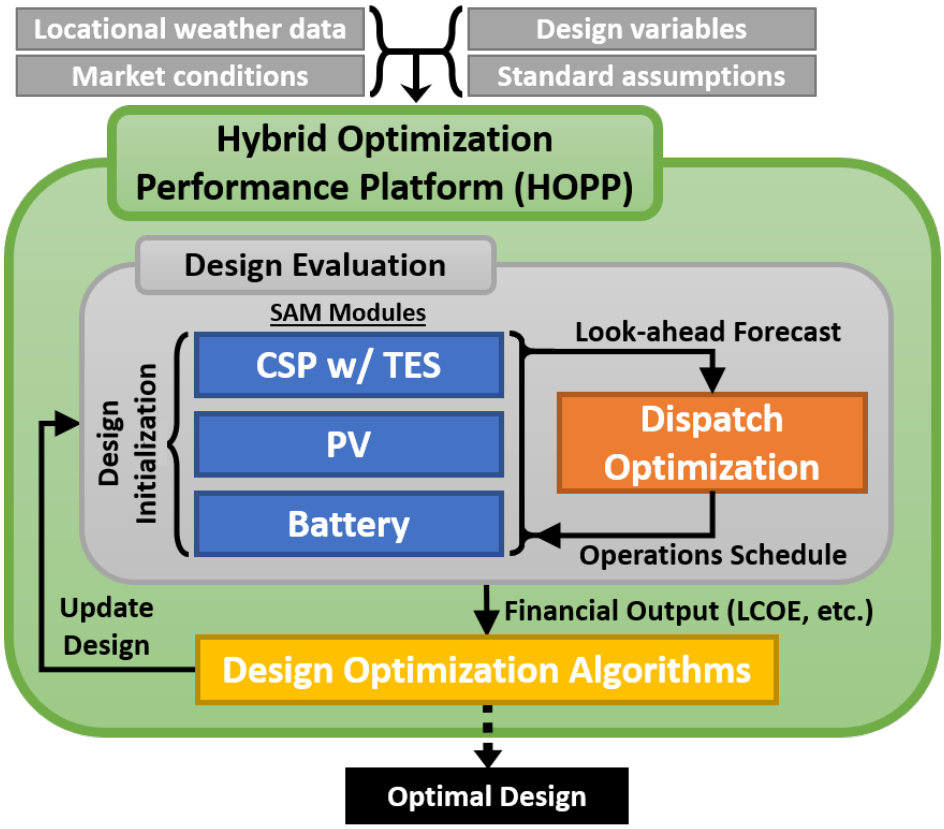

Figure 3. Overview of the HOPP software framework: price-taker dispatch optimization governs time-dependent subsystem operations, and nonlinear optimization algorithms are used to determine the optimal value of high-level design and sizing variables.

In the following sub-sections, we describe (i) the methods for integrating tower and trough CSP configurations into the HOPP framework, (ii) the dispatch optimization model within HOPP, (iii) simulation clustering techniques to reduce computational expense, and (iv) design analysis methods available through HOPP.

2.1 Integration of CSP into HOPP

At the core of HOPP's design evaluation exists the System Advisor Model (SAM) technology and financial modules. Note that wind generation is also available through HOPP. However, it is not presented here because the focus of this work is on CSP-PV-battery hybrids. HOPP uses NREL-PySAM, a Python application programming interface (API) for SAM (NREL 2022), to interface with all technology performance and financial modules available through HOPP except for the CSP technology performance models.

The CSP technology models use PySSC, which is the Python API for interacting with the SAM Simulation Core (SSC). HOPP's CSP tower configuration uses SAM's molten-salt power tower technology model, and the trough configuration uses the physical parabolic trough model. We use PySSC rather than PySAM because it includes recently developed modeling capabilities that are required for integration with HOPP but are not yet available within the officially released versions of PySAM. Specifically, these capabilities allow the CSP technology performance models to be evaluated using externally generated dispatch control signals, with user-specified initial states for all components. We hope to merge the required capabilities into SSC's *develop* branch in the near future, which would enable the use of PySAM.

Currently, only SAM's *single owner* financial model is available within HOPP, which assumes that the project owner builds, owns, and operates the power system and has sufficient tax liability to fully utilize all tax benefits. The owner may be either the original developer or a third-party tax investor that purchases the project from the developer.

2.1.1 Annual Performance Simulation

Figure 4 presents the information flow for the evaluation of a hybrid system involving CSP and battery technologies, specifically focusing on a tower CSP configuration. When a hybrid configuration with CSP and/or battery storage is simulated, this information flow occurs within the *HybridSimulation* class. For tower CSP configurations, SSC uses SolarPILOT™ to generate the heliostat field layout based on the provided receiver thermal rating, tower height, receiver height and diameter. Additionally, HOPP can invoke SolarPILOT's optimization method to optimize the heliostat field layout, tower height, receiver height, and receiver diameter for a given receiver thermal rating, target peak solar flux constraint, solar resource, and cost assumptions. The SolarPILOT and SAM documentation contain more detail on this optimization (Wagner and Wendelin 2018). This step is skipped if the parabolic trough CSP configuration is used. For the parabolic trough configuration, SAM handles the selection of solar field piping diameters based on the number of field subsections, field thermal rating, and flow conditions (Wagner and Gilman 2011).

Hybrid dispatch optimization decisions do not influence the performance of the PV solar field, i.e., control signals related to battery operations do not propagate back to the PV system operation and do not change the initial prediction PV system performance. As a result, the entire year simulation for PV performance is executed before invoking the simulation with dispatch optimization. Wind farms are modeled similarly within HOPP; however, there is ongoing work to use more detailed wind models, e.g., FLORIS, that can accept control signals to curtail turbine power by yaw and induction control (NREL 2021). Future work could enable more controllable PV performance models allowing inverter control and/or tilt control for tracking systems. This update would require the PV performance model to be executed within the dispatch optimization loop.

Before the simulation with dispatch optimization begins, the CSP performance models are called to predict the time series available CSP solar field and receiver thermal energy generation. This forecast of the maximum possible CSP thermal energy production is accomplished by executing SSC with approximately unlimited TES capacity and very low receiver startup time and energy requirements. The time series of available thermal energy generation from the solar field is an important input to the dispatch optimization model, and is used by the dispatch optimization model to make decisions about CSP collection operations and the expected energy generation as a result of these operations. During this forecasting of CSP thermal generation, HOPP also gathers and stores the power cycle efficiency table from SSC, which will be used within the dispatch optimization model to simulate off-design performance of the CSP cycle. After completing this forecasting, the original parameter values are reapplied to SSC in preparation for the simulation with the dispatch optimization loop.

The last process handled by HOPP before the simulation with dispatch optimization loop is the calculation of system installation cost. By default, HOPP models installed cost for PV, wind, and battery technologies rather simplistically. PV and wind installed costs scale with technology power output, i.e., $/MW. Battery technology assumes installed

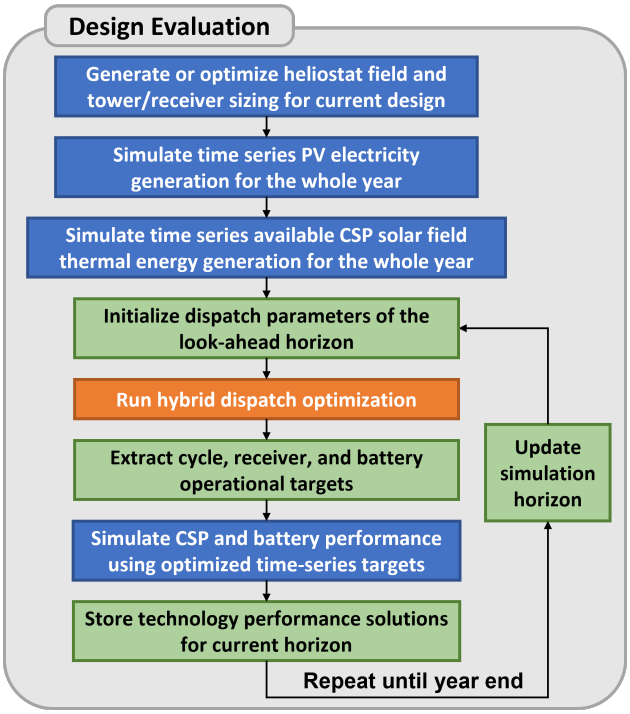

Figure 4. Information flow for design performance evaluation for a hybrid system involving CSP and battery technologies, specifically focusing on tower CSP configuration.

costs scale with both rated power and capacity, i.e., $/MW and $/MWh. However, HOPP could be modified to include more complex cost calculators as the user sees fit. For CSP systems, system costs do not scale linearly, and do not scale with only the power generation capacity of CSP plant (power cycle rated output); therefore, the installed cost calculation within HOPP mimics the CSP technology *System Costs* page of SAM (National Renewable Energy Laboratory 2021). These system costs as well as all of HOPP's financial parameters can be modified as required for the analysis use case.

To simulate the performance of a hybrid system with storage assets, HOPP uses price-taker dispatch optimization to make operational decisions about charging and discharging storage. This process is done using a rolling time horizon approach to step through the year with a dispatch look-ahead horizon and roll-forward simulation horizon (or the frequency of dispatch re-optimization). By default, HOPP uses a 48-hour dispatch look-ahead horizon and a 24-hour roll-forward simulation horizon. At the beginning of the performance simulation, the hybrid dispatch optimization model is built and parameters are initialized depending on the technologies within the system (described in detail in Section 2.2). The dispatch optimization model is solved using one of the open-source or commercial solvers available through HOPP. After convergence, the operational targets for the CSP cycle, CSP receiver, and battery are extracted from the portion of the dispatch solution coinciding with the roll-forward simulation horizon and are passed to the respective technology performance models. The performance models simulate CSP and battery performance using control signals derived from the dispatch solution for optimal operations, and the time-series results are collected and stored within HOPP's class structure. The simulation horizon and dispatch parameters are updated, and the process is repeated until the end of the annual simulation.

After the annual performance simulation, system performance information is propagated to the financial models, which are executed to provide the techno-economic assessment of the hybrid system under the assumed conditions.

2.1.2 Parameter Scaling

Within SAM's CSP tower and trough technology models there exists a small subset of parameters that are absolute values and not intrinsically set up to scale with system sizing. As a result, solutions with poor technology performance can be encountered due to an unrealistic set of input parameters. These parameters can be set to realistic

values by the user for any single set of design parameters, but ideally should also scale automatically during automated sampling or optimization within a wide parameter space of possible system capacity. To address this, we created methods to scale these parameters depending on the high-level system design parameters used to size the CSP systems, i.e., hours of TES, solar multiple, and power cycle capacity. The model parameters that are specified with absolute values within SAM, but are currently set up in HOPP to optionally scale with CSP sizing, are as follows: (i) TES tank heaters, (ii) tank height, (iii) heliostat sizing, (iv) heliostat parasitic power requirements, and (v) receiver tube diameter. The first two parameters are scaled for both tower and trough systems while the last three are only applicable in tower CSP configurations. This parameter scaling can be toggled on and off through the HOPP interface depending on user needs.

In the TES model, used by both tower and trough configurations, there exist cold and hot tank heater capacities. The purpose of these heaters is to recover molten salt temperature if the temperature falls below a specified set point. We assume these heater capacities scale linearly with TES capacity relative to the values specified in the SAM default molten-salt power tower and physical trough models, respectively.

The TES model requires the user to supply an assumed tank height. In HOPP's parameter scaling method, we assume the TES tank height scales with TES capacity to maintain a constant height-to-diameter aspect ratio. Unfortunately, this assumption breaks down when TES capacity increases to the point where multiple tanks could be the most economic solution. Future work could investigate this transition point and apply a method for scaling the TES system to use multiple tank pairs in parallel, which would provide the system the benefit of tank redundancy.

As receiver thermal rating decreases, the receiver height and diameter must also decrease to minimize heat loss subject to the maximum incoming solar flux limit. Similarly, as the receiver thermal rating increases, the receiver height and diameter must increase to avoid exceeding limits on solar flux concentration. High levels of spillage can occur if the heliostat size is larger than the receiver intercepting surface. To address this, we scale heliostat width and height (assumed to be a square) based on an approximate receiver area, which is estimated using the design point receiver thermal rating, allowable peak flux concentration, and an assumed average-to-peak flux ratio of 0.65. The heliostat size is then set to 70% of the estimated height or width of the receiver. Heliostat costs are implemented simply via a $\$/m^2$ metric that is independent of heliostat size, and thus this scaling is only intended to reduce spillage loss to reasonable levels and thereby avoid artificially penalizing small-capacity designs. It is not intended to capture trade-offs in capital or operational costs of small versus large heliostats. This is just one approach to scale the heliostat sizing with varying receiver sizes, and there may exist more comprehensive approaches to scaling heliostat sizing.

We assume heliostat startup energy and tracking power scale linearly with heliostat reflective area relative to the default startup energy, tracking power, and heliostat size that exist in the SAM default molten-salt power tower case. This is a simple approximation as these values would realistically scale with the rotational inertia of the heliostat about the elevation and azimuth axes. However, this would require more knowledge about the specific heliostat design.

Lastly, we scale the receiver tube diameter to achieve a target velocity at design point mass flow rate. We assume a tube internal target velocity of 3.5 m/s. This maintains turbulent flow conditions through the receiver during reduced flow conditions, and avoids unrealistically high flow velocities and pumping parasitic loads for cases with a large receiver thermal capacity.

2.1.3 Capacity Value

One potential revenue stream for future renewable energy systems with storage is capacity payments. Capacity payments can be provided to a power plant by the utility based on numerous market-specific rules and qualifications. Within HOPP, we provide a *capacity basis* option where the annual capacity payment is calculated as the product of the capacity payment amount ($/kW-yr), system nameplate capacity (kW), and "eligible" percent of nameplate (%) or *capacity credit*. Numerous methods have been proposed for estimating the capacity credit for CSP systems or other energy storage resources (Sioshansi, Madaeni, and Denholm 2014; Madaeni, Sioshansi, and Denholm 2012). These methods span everything from a fixed credit depending on capacity of storage assets (Denholm and Margolis 2018), to methods that use historic or simulated generation profiles to calculate capacity credit using a subset of

hours characterized by high loss-of-load probability or, more simplistically, high net load or high price (Sioshansi, Madaeni, and Denholm 2014).

Here, we adopt one simple method for calculating capacity credit for implementation within HOPP. The HOPP capacity credit calculation follows a method similar to that presented by Jorgenson, Denholm, and Mehos (2014). In this method, the credit is based on either the system's generation or the combination of generation and available storage during a subset of time periods. HOPP allows the user to provide a time series of boolean values to specify which hours of the year are to be used in the capacity credit calculation. This approach provides the greatest flexibility to the HOPP user in determining which set of periods to select. For example, this time series could be based on the *X* highest net-load hours within the year given expected load and variable renewable generation at the hybrid system location, or based on a fixed schedule of, for example, 5 p.m. to 9 p.m. for weekdays in summer months. Additionally, we assume that the hybrid system operator (i.e., the dispatch optimization model) has no prior knowledge about which hours qualify for capacity payments, and thus the generation of electricity or accumulation of storage within these hours is not explicitly incentivized when determining the optimal operational schedule. This approach is consistent with a scenario where the utility uses the plant's historical generation data to calculate capacity payments.

Given a schedule of qualifying periods, HOPP can calculate capacity credit based on only the system's generation profile, or based on the generation profile plus available storage (less CSP power cycle startup requirements if the power cycle is not already operating). The former works well if the qualifying periods coincide with periods that are incentivized within the dispatch optimization model through high electricity prices or required load. The latter approach provides a method to evaluate if the storage asset could respond if called upon by the utility, assuming it is not already generating. However, the latter method does not deduct energy from storage during those periods in which it is possible to increase output, and thus may overestimate storage availability in later periods. These methods and the results they provide should be used with caution because a hybrid system could achieve a low capacity credit while generating high system operating revenue if the dispatch incentives and periods contributing to capacity credit do not coincide.

2.2 Dispatch Optimization

Unlike traditional non-dispatchable renewable energy systems, energy storage assets require operational decisions that maximize the value of the asset, e.g., when and at what rate to charge and discharge the asset. To address this, we implement a mixed integer linear program (MILP) dispatch optimization model that either (i) maximizes the hybrid system *gross profit* while accounting for operational costs or (ii) minimizes system operating cost while load following. The dispatch model, hereafter referred to as ($\mathscr{H}$), is written in Pyomo which is a Python-based, open-source optimization modeling language developed by Sandia National Laboratories (Hart et al. 2017).

Within the HOPP framework, we use a modular approach to build a dispatch model depending on the technologies within the hybrid system of analysis, shown in Figure 5. Each technology module is a self-contained Pyomo dispatch model that is specific to the decisions required by the technology the module is representing. These modules are connected to a central model via Pyomo *arcs* and *ports*. By implementing HOPP's dispatch optimization methods using this modular approach, we gain significant advantages over a monolith modeling approach: (i) each module is self-contained, which eases the burden of understanding, modifying, and/or debugging the module and (ii) ports provide a uniform interface between the technology module and the central model, which enables the development of interchangeable modules for the same technology, i.e., a different set of parameters, variables, and/or constraints that allows for various levels of detail within the dispatch module.

The dispatch optimization model, ($\mathscr{H}$), uses temporal discretization to model operational decisions over a look-ahead horizon. For each technology dispatch module, we use Pyomo's *Block* components to create a set of constraints for a single time period. These technology blocks are repeated for the set of time periods that the dispatch model is representing. For energy storage technologies, these time blocks must be linked through constraints that require the state-of-charge at the beginning of a time block is equal to the state-of-charge at the end of the previous time block. This modeling methodology provides flexibility in the future to construct a monolith dispatch model with varying duration and fidelity time blocks.

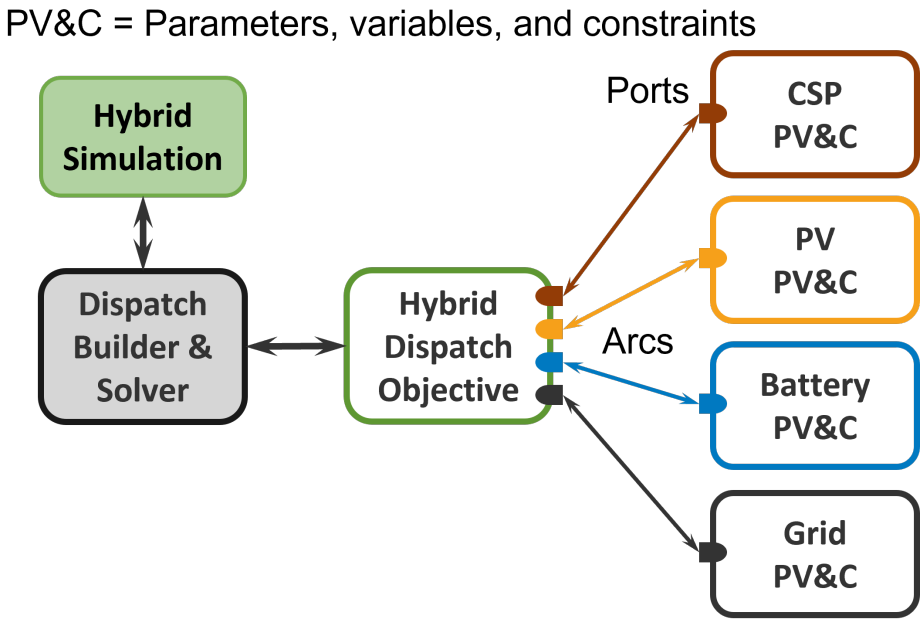

Figure 5. HOPP hybrid simulation dispatch optimization module approach.

2.2.1 Mathematical Formulation

Given the modular structure of our model (highlighted in Figure 5), we present the mathematical formulation for each technology module and then present the hybrid dispatch objective as a whole using color coding to highlight the addition of each technology module. This method of documentation more closely aligns with the implementation of this dispatch model within the HOPP software framework. The combination of these technology dispatch modules as a whole, ($\mathscr{H}$), is a modified version of the dispatch optimization model from Hamilton et al. (2020). As a result, we borrow much of the notation used in this reference.

The dispatch model, ($\mathscr{H}$), uses a look-ahead time horizon that consists of a set of time periods referred to as τ. Currently, HOPP is designed for hourly time fidelity; however, the dispatch model, ($\mathscr{H}$), can be modified to handle sub-hourly time periods. We present each technology dispatch model using the subscripts t and $t-1$ to represent the current and previous time periods, respectively. By using Pyomo blocks for the set of time periods, τ, all of the problem parameters and variables can be indexed by time; however, we assume a majority of the problem parameters are constant with respect to time, which we present as parameter notation without a subscript t. Conversely, parameters that are indexed by time are presented with the subscript t.

The following formulation, ($\mathscr{H}$), requires the initial operational state of the system, PV field and receiver energy generation forecasts, the expected cycle conversion efficiency profile as a function of ambient temperature and thermal input, and the energy price or desired load profile depending on the system analysis. Initialization parameters used to set variable values at $t = 0$ follow variable notation and are not included here. Variables and parameters describe energy (thermal MWh_t or electric MWh_e) states and power flows (thermal MW_t or electric MW_e) in the system. We use lowercase letters to represent variables and capital letters for parameters. All binary variables are represented with some variant of the letter y.

Concentrating solar power with thermal energy storage

Table 1 and Table 2 present the CSP technology dispatch module parameters and variables, respectively.

Table 1. Parameters for the CSP technology dispatch module.

CSP Field and Receiver Parameters		
C^{rec}	Generation cost for the CSP field and receiver	[\$/MWh$_t$]
C^{rsu}	Fixed cost for receiver startup	[\$/start]
Δ^l	Minimum time to start the receiver	[hr]
Δ_t^{rs}	Estimated fraction of time period t required for receiver startup	[-]
E^{hs}	Heliostat field startup or shut down parasitic loss	[MWh$_e$]
E^r	Required energy expended to start receiver	[MWh$_t$]
L^r	Receiver pumping power per unit power produced	[MW$_e$/MW$_t$]
Q_t^{in}	Available thermal power generated by the CSP heliostat field in time t	[MW$_t$]
Q^{rl}	Minimum operational thermal power delivered by receiver	[MW$_t$]
Q^{ru}	Allowable power per period for receiver startup	[MW$_t$]
W^h	Heliostat field tracking parasitic loss	[MW$_e$]
Power Cycle Parameters		
C^{pc}	Generation cost for power cycle operation	[\$/MWh$_e$]
C^{csu}	Fixed cost for power cycle startup	[\$/start]
$C^{\delta x}$	Penalty for change in power cycle thermal input	[\$/ΔMW$_t$]
η_t^{amb}	Cycle efficiency ambient temperature adjustment factor in time t	[-]
η_t^c	Normalized condenser parasitic loss in time t	[-]
E^c	Required energy expended to start cycle	[MWh$_t$]
η^{des}	Cycle nominal efficiency	[-]
η^p	Slope of linear approximation of power cycle performance curve	[MW$_e$/MW$_t$]
L^c	Cycle heat transfer fluid pumping power per unit energy expended	[MW$_e$/MW$_t$]
Q^c	Allowable power per period for cycle startup	[MW$_t$]
Q^l	Minimum operational thermal power input to cycle	[MW$_t$]
Q^u	Maximum operational thermal power input to cycle	[MW$_t$]
W^u	Cycle electric power rated capacity	[MW$_e$]
TES and Miscellaneous Parameters		
Δ	Time step duration	[hr]
E^u	Thermal energy storage capacity	[MWh$_t$]

Table 2. Variables for the CSP technology dispatch module.

Continuous		
s_t	TES reserve quantity at time t	[MWh_t]
u_t^{csu}	Cycle startup energy inventory at time t	[MWh_t]
u_t^{rsu}	Receiver startup energy inventory at time t	[MWh_t]
$\dot{w}_t$	Power cycle electricity generation at time t	[MW_e]
$\dot{w}_t^l$	Electrical load of CSP system at time t	[MW_e]
x_t	Cycle thermal power utilization at time t	[MW_t]
x_t^{δ}	Power cycle change in thermal power input at time t	[MW_t]
x_t^r	Thermal power delivered by the receiver at time t	[MW_t]
x_t^{rsu}	Receiver startup power consumption at time t	[MW_t]
Binary		
y_t	1 if cycle is generating electric power at time t; 0 otherwise	
y_t^{csu}	1 if cycle is starting up at time t; 0 otherwise	
y_t^{csup}	1 if cycle cold startup penalty is incurred at time t (from off); 0 otherwise	
y_t^r	1 if receiver is generating "usable" thermal power at time t; 0 otherwise	
y_t^{rsu}	1 if receiver is starting up at time t; 0 otherwise	
y_t^{rsup}	1 if receiver cold startup penalty is incurred at time t (from off); 0 otherwise	

Receiver Operations:

We include the following constraints that govern receiver operations:

Receiver startup

$$u_t^{rsu} \leq u_{t-1}^{rsu} + \Delta x_t^{rsu} \qquad \forall\, t \in \tau : t \geq 2 \tag{2.1a}$$

$$u_t^{rsu} \leq E^r y_t^{rsu} \qquad \forall\, t \in \tau \tag{2.1b}$$

$$y_t^r \leq \frac{u_t^{rsu}}{E^r} + y_{t-1}^r \qquad \forall\, t \in \tau : t \geq 2 \tag{2.1c}$$

$$y_t^{rsu} + y_{t-1}^r \leq 1 \qquad \forall\, t \in \tau : t \geq 2 \tag{2.1d}$$

$$x_t^{rsu} \leq Q^{ru} y_t^{rsu} \qquad \forall\, t \in \tau \tag{2.1e}$$

$$y_t^{rsu} \leq \frac{Q_t^{in}}{Q^{rl}} \qquad \forall\, t \in \tau \tag{2.1f}$$

$$y_t^{rsup} \geq y_t^{rsu} - y_{t-1}^{rsu} \qquad \forall\, t \in \tau : t \geq 2 \tag{2.1g}$$

Receiver Supply and Demand

$$x_t^r + x_t^{rsu} \leq Q_t^{in} \qquad \forall\, t \in \tau \tag{2.2a}$$

$$x_t^r \leq Q_t^{in} y_t^r \qquad \forall\, t \in \tau \tag{2.2b}$$

$$x_t^r \geq Q^{rl} y_t^r \qquad \forall\, t \in \tau \tag{2.2c}$$

$$y_t^r \leq \frac{Q_t^{in}}{Q^{rl}} \qquad \forall\, t \in \tau \tag{2.2d}$$

Constraint (2.1a) accounts for receiver startup energy "inventory," which can assume a positive value during time periods of receiver startup (Constraint (2.1b)). Power production assumes a positive value only upon completion of a startup or if the receiver also operates in the time period prior (Constraint (2.1c)). In the latter case, the receiver cannot be starting up in the next time period (Constraint (2.1d)). Ramp-rate limits hold during the startup procedure (Constraint (2.1e)). The presence of trivial solar resource prevents receiver startup (Constraint (2.1f)). Constraints (2.1g) ensure that penalties for receiver startup are incurred.

The parameter Q_t^{in} serves as an upper bound on the thermal power produced by the receiver, from which any energy used for startup detracts (Constraint (2.2a)). Constraints (2.2b) and (2.2c) permit the receiver to generate thermal power within the specified upper and lower bounds, respectively, and only in power-producing mode. Receiver thermal power generation is subject to a lower bound by Constraint (2.2c). The receiver cannot operate (Constraint (2.2d)) in the absence of thermal power.

Power Cycle Operations:

Power cycle operation constraints are similar to those of receiver operations:

Cycle startup

$$u_t^{csu} \leq u_{t-1}^{csu} + \Delta Q^c y_t^{csu} \qquad \forall\, t \in \tau : t \geq 2 \qquad (2.3a)$$

$$u_t^{csu} \leq E^c y_t^{csu} \qquad \forall\, t \in \tau \qquad (2.3b)$$

$$y_t \leq \frac{u_t^{csu}}{E^c} + y_{t-1} \qquad \forall\, t \in \tau : t \geq 2 \qquad (2.3c)$$

$$y_t^{csu} + y_{t-1} \leq 1 \qquad \forall\, t \in \tau : t \geq 2 \qquad (2.3d)$$

$$y_t^{csup} \geq y_t^{csu} - y_{t-1}^{csu} \qquad \forall\, t \in \tau : t \geq 2 \qquad (2.3e)$$

Power Supply and Demand

$$x_t + \frac{E^c}{\Delta} y_t^{csu} \leq Q^u \qquad \forall\, t \in \tau \qquad (2.4a)$$

$$x_t \leq Q^u y_t \qquad \forall\, t \in \tau \qquad (2.4b)$$

$$x_t \geq Q^l y_t \qquad \forall\, t \in \tau \qquad (2.4c)$$

$$\dot{w}_t = \frac{\eta_t^{amb}}{\eta^{des}} [\eta^p x_t + (W^u - \eta^p Q^u) y_t] \qquad \forall\, t \in \tau \qquad (2.4d)$$

$$x_t^{\delta} \geq x_t - x_{t-1} \qquad \forall\, t \in \tau : t \geq 2 \qquad (2.4e)$$

$$\dot{w}_t^l = \eta_t^c \dot{w}_t + L^r (x_t^r + x_t^{rsu}) + L^c (x_t + Q^c y_t^{csu}) + W^h y_t^r + \frac{E^{hs}}{\Delta} y_t^{rsu} \qquad \forall\, t \in \tau \qquad (2.4f)$$

Constraint (2.3a) accounts for startup energy "inventory," which can only be positive during time periods in which the cycle is starting up (Constraint (2.3b)). Normal cycle operation can occur upon completion of startup energy requirements or if the cycle is operating normally in the prior time period (Constraint (2.3c)). In the latter case, the cycle cannot start up in the time period directly following operation (Constraint (2.3d)). Cycle start up penalties are incurred via Constraint (2.3e).

Constraint (2.4a) limits the cycle input thermal power during periods when the cycle is starting up. This is a model approximation to derate power cycle output during startup periods. In reality, the cycle power output is not derated, but the total energy production during the time period is reduced due to the startup during the period. Constraints (2.4b) and (2.4c) provide analogous restrictions on power cycle operation to those of (2.2b) and (2.2c), respectively. The relationship between electrical power and cycle heat input is modeled as a linear function with corrections for ambient temperature effects (Constraint (2.4d)). Constraint (2.4e) measures the positive change in cycle thermal input, i.e., ramping, over time. Constraint (2.4f) calculates the CSP system load depending operational decisions.

TES Energy Balance State of Charge

The system's energetic state implies power terms that can assume either sign; the thermal storage charge state (s_t) reconciles their difference. We therefore impose some additional constraints with respect to TES state of charge:

$$s_t - s_{t-1} = \Delta[x_t^r - (Q^c y_t^{csu} + x_t)] \qquad \forall\, t \in \tau : t \geq 2 \qquad (2.5a)$$

$$s_t \leq E^u \qquad \forall\, t \in \tau \qquad (2.5b)$$

$$s_{t-1} \geq \Delta \cdot \Delta_t^{rs}[Q^u(-3 + y_t^{rsu} + y_{t-1} + y_t) + x_t] \qquad \forall\, t \in \tau : t \geq 2 \qquad (2.5c)$$

Constraint (2.5a) balances energy to and from TES with the charge. Constraint (2.5b) imposes the upper bound to TES charge state. If the power cycle is operating in time periods $t-1$ and t, and if the receiver is starting up in time t, then there must be a sufficient charge level in the TES in time $t-1$ to ensure that the power cycle can operate through its startup period (Constraint (2.5c)). Constraint (2.5c) uses Q^u as a big-M value to make the constraint non-binding when the specific condition is not occurring, i.e., either the cycle is not operating or the receiver is not starting up in the period. The expected fraction of a time period used for receiver startup is given by (2.6), if applicable.

$$\Delta_t^{rs} = \min\left\{1, \max\left\{\Delta^l, \frac{E^r}{\max\left\{\varepsilon, Q_t^{in}\Delta\right\}}\right\}\right\} \qquad (2.6)$$

Constraints (2.5a)–(2.5c) measure TES state of charge via energy flow.

Variable bounds

Variable bounds are enforced in (2.7a) and (2.7b).

$$s_t,\, u_t^{csu},\, u_t^{rsu},\, \dot{w}_t,\, \dot{w}_t^l,\, x_t,\, x_t^{\delta},\, x_t^r,\, x_t^{rsu} \geq 0 \qquad \forall\, t \in \tau \qquad (2.7a)$$

$$y_t,\, y_t^{csu},\, y_t^{csup},\, y_t^r,\, y_t^{rsu},\, y_t^{rsup} \in \{0,1\} \qquad \forall\, t \in \tau \qquad (2.7b)$$

Photovoltaic field

Due to the PV systems not having energy storage, the PV technology dispatch module is very simplistic compared to the CSP module. The PV dispatch model can choose to either take PV generation, sending it to either the grid or battery storage, or curtail any amount of the available PV generation during the time period. Table 3 presents the PV technology dispatch module parameters and variables.

Table 3. PV dispatch module parameters and variables.

PV Field Parameters		
C^{pv}	Generation cost of PV field	[\$/MWh$_e$]
Δ	Time step duration	[hr]
W_t^{pv}	Available PV (AC) generation in time t	[MW$_e$]
PV Field Variables		
$\dot{w}_t^{pv}$	PV generation in time t	[MW$_e$]

PV Constraints:

$$\dot{w}_t^{pv} \leq W_t^{pv} \qquad \forall\, t \in \tau \qquad (2.8a)$$

$$\dot{w}_t^{pv} \geq 0 \qquad \forall\, t \in \tau \qquad (2.8b)$$

Within the hybrid framework, we assume that the PV system has a *take it or leave it* policy in which the hybrid system can take up to the available generation at any time (Constraint (2.8a)) or curtail part or all of the available generation depending on other system constraints. Non-negativity is enforced by Constraint (2.8b).

Battery

Table 4 presents the electric battery technology dispatch module parameters and variables.

Table 4. Battery dispatch module parameters and variables.

Battery Parameters		
C^{bc}, C^{bd}	Operating cost of charging and discharging battery	[\$/MWh$_e$]
C^{bl}	Lifecycle cost for battery	[\$/lifecycle]
C^B	Battery manufacturer-specified capacity	[MWh$_e$]
Δ	Time step duration	[hr]
η^+, η^-	Charge and discharge efficiency	[-]
$\underline{P}^B, \overline{P}^B$	Battery minimum and maximum power ratings	[MW$_e$]
$\underline{S}^B, \overline{S}^B$	Battery state of charge minimum and maximum operational bounds	[-]
Battery Variables		
b^c	Battery cycle count	[-]
b_t^{soc}	State of charge of battery in time period t	[-]
$\dot{w}_t^+, \dot{w}_t^-$	Power into and out of the battery at time t	[MW$_e$]
y_t^+, y_t^-	1 if battery is charging or discharging in time period t; 0 otherwise	

Battery Constraints:

$$b_t^{soc} = b_{t-1}^{soc} + \Delta\left(\frac{\eta^+ \cdot \dot{w}_t^+ - \frac{\dot{w}_t^-}{\eta^-}}{C^B}\right) \qquad \forall\, t \in \tau : t \geq 2 \tag{2.9a}$$

$$\underline{S}^B \leq b_t^{soc} \leq \overline{S}^B \qquad \forall\, t \in \tau \tag{2.9b}$$

$$\underline{P}^B y_t^- \leq \dot{w}_t^- \leq \overline{P}^B y_t^- \qquad \forall\, t \in \tau \tag{2.9c}$$

$$\underline{P}^B y_t^+ \leq \dot{w}_t^+ \leq \overline{P}^B y_t^+ \qquad \forall\, t \in \tau \tag{2.9d}$$

$$y_t^+ + y_t^- \leq 1 \qquad \forall\, t \in \tau \tag{2.9e}$$

$$b^c \geq \frac{\Delta}{C^B} \sum_{t \in \tau} \dot{w}_t^- \tag{2.9f}$$

Constraint (2.9a) reconciles battery state-of-charge in each period according to the charging and discharging decisions in that period and the previous period's state-of-charge. Battery state-of-charge is bounded both below and above (Constraint (2.9b)). Power flow into and out of the battery is bounded by Constraints (2.9c) and (2.9d). In this formulation, it is assumed that the charging and discharging power limits are identical; however, this model can be updated to handle dissimilar limits. The battery cannot be charging and discharging simultaneously (Constraint (2.9e)), while Constraint (2.9f) measures battery cycle count similar to what is done in Scioletti et al. 2017.

Variable bounds are enforced in (2.10a) and (2.10b).

$$b^c,\ b_t^{soc},\ \dot{w}_t^+,\ \dot{w}_t^- \geq 0 \qquad \forall\, t \in \tau \tag{2.10a}$$

$$y_t^+,\ y_t^- \in \{0,1\} \qquad \forall\, t \in \tau \tag{2.10b}$$

Electric power grid

Table 5 presents the electric grid dispatch module parameters and variables.

Grid Constraints:

Table 5. Electric grid dispatch module parameters and variables.

Grid Parameters		
Δ	Time step duration	[hr]
ε	Small value used in objective for binary logic	[$]
P_t^s, P_t^p	Electricity sale and purchase price in time t	[$/MWh$_e$]
W_t^g, W_t^l	Grid transmission limit for generation and load in time t	[MW$_e$]
Grid Variables		
$\dot{w}_t^{sg}, \dot{w}_t^{sl}$	System generation and load in time t	[MW$_e$]
$\dot{e}_t^s, \dot{e}_t^p$	Electricity sold to and purchased from grid in time t	[MW$_e$]
y_t^g	1 if system is net generating in time period t; 0 otherwise	

$$\dot{e}_t^s - \dot{e}_t^p = \dot{w}_t^{sg} - \dot{w}_t^{sl} \qquad \forall\, t \in \tau \tag{2.11a}$$

$$\dot{e}_t^s \leq W_t^g y_t^g \qquad \forall\, t \in \tau \tag{2.11b}$$

$$\dot{e}_t^p \leq W_t^l (1 - y_t^g) \qquad \forall\, t \in \tau \tag{2.11c}$$

Constraint (2.11a) provides an energy balance at the transmission interconnect of the hybrid system. Electricity sales are limited by the transmission limit for generation during periods in which the system is generating net power (Constraint (2.11b)). During periods where the hybrid system net generation is negative, Constraint (2.11c) limits the load the system can draw from the grid.

Variable bounds are enforced in (2.12a) and (2.12b).

$$\dot{w}_t^{sg},\ \dot{w}_t^{sl},\ \dot{e}_t^s,\ \dot{e}_t^p \geq 0 \qquad \forall\, t \in \tau \tag{2.12a}$$

$$y_t^g \in \{0, 1\} \qquad \forall\, t \in \tau \tag{2.12b}$$

Hybrid system

Within the hybrid dispatch module, we combine all of the individual technology dispatch models to create the master hybrid dispatch model ($\mathscr{H}$). Currently, the hybrid dispatch module can be constructed using one of two objective functions: (i) maximize gross profit, ($\mathscr{H}_1$), or (ii) minimize load following operating cost, ($\mathscr{H}_2$). The former objective uses time varying electricity prices to maximize the hybrid system gross profit by dispatching storage assets during time periods of high value and charging storage assets during time periods of over-generation or low value prices. The latter objective employs a user-defined load profile and dispatches the hybrid system to try to meet said load profile using the lowest-operating-cost solution of available technologies. This approach could be used for a remote system that must cover a load requirement or an entity looking to size a system that dispatches in a restrictive manner.

The hybrid dispatch module introduces no new variables and minimal new parameters as shown in Table 6. In the presentation of these objective functions, we have color coded the individual technology dispatch module parameters and variables to explicitly identify their contributions to the objective. We use the same color code scheme presented in Figure 5 but have repeated them here for reader convenience: CSP, PV, Battery, Grid, and Hybrid.

Table 6. Hybrid dispatch module parameters.

Hybrid Parameter		
γ	Exponential time weighting factor	[-]

Maximize Gross Profit Objective:

This objective for the dispatch model ($\mathscr{H}_1$) is to maximize gross profit or electricity sales less system operating costs during the time horizon.

$$
\begin{aligned}
(\mathscr{H}_1)\ \text{maximize}\quad & \sum_{t\in\tau}\Bigg[\Delta\left(\gamma^t P_t^s \dot{e}_t^s - \left(\frac{1}{\gamma}\right)^t P_t^p \dot{e}_t^p\right) - \varepsilon y_t^g \\
& - \left(\frac{1}{\gamma}\right)^t \left(\Delta C^{rec} x_t^r + C^{rsu} y_t^{rsup} + \Delta C^{pc} \dot{w}_t + C^{csu} y_t^{csup} + C^{\delta x} x_t^{\delta}\right) \\
& - \left(\frac{1}{\gamma}\right)^t \Delta C^{pv} \dot{w}_t^{pv} \\
& - \left(\frac{1}{\gamma}\right)^t \Delta\left(C^{bc} \dot{w}_t^{+} + C^{bd} \dot{w}_t^{-}\right)\Bigg] - C^{bl} b^c
\end{aligned} \tag{2.13}
$$

where Δ across all dispatch modules are equal.

Minimize Load Following Operating Cost Objective:

This objective ($\mathscr{H}_2$) is to minimize system operating costs while load following. For this objective function, the dispatch model uses the time varying transmission limit parameter in the grid module, W_t^g, to enforce the desired load profile as the system's generation upper bound. This approach means that the hybrid system cannot generate more electricity than the desired load profile specifies at any given time period. Therefore, this approach can result in a hybrid system that severely underproduces compared to the same hybrid configuration with the objective to maximize gross profit.

This formulation uses the electricity selling price, P_t^s, to penalize the system for missing load, i.e., the hybrid system dispatch wants to minimize the difference between electricity sold and the desired load profile (transmission limit). Additionally, this formulation incentivizes storage charging (note the negative contribution to the objective for CSP receiver collection and battery charging) to enable the system to meet load during hours that may not be within the dispatch time horizon. This approach provides a maximum storage charge when resources are available to minimize unmet load in the future.

$$
\begin{aligned}
(\mathscr{H}_2)\ \text{minimize}\quad & \sum_{t\in\tau}\Bigg[\Delta\gamma^t\left(P_t^s\left(W_t^g - \dot{e}_t^s\right) + P_t^p \dot{e}_t^p\right) + \varepsilon y_t^g \\
& + \gamma^t\left(-\Delta C^{rec} x_t^r + C^{rsu} y_t^{rsup} + \Delta C^{pc} \dot{w}_t + C^{csu} y_t^{csup} + C^{\delta x} x_t^{\delta}\right) \\
& + \gamma^t \Delta C^{pv} \dot{w}_t^{pv} \\
& + \gamma^t \Delta\left(-C^{bc} \dot{w}_t^{+} + C^{bd} \dot{w}_t^{-}\right)\Bigg] + C^{bl} b^c
\end{aligned} \tag{2.14}
$$

Δ across all dispatch modules are equal. This objective function is a relatively new capability at the time of writing this report and should be used with caution. Because the load profile is imposed on the system, dispatching using this objective can result in large amounts of curtailment or under-utilized assets, which results in worsened system financial metrics.

Hybrid Constraints:

The hybrid dispatch module houses some system level constraints that further interconnect the individual technology dispatch modules.

$$\dot{w}_t^{sg} = \dot{w}_t + \dot{w}_t^{pv} + \dot{w}_t^{-} \qquad \forall\, t \in \tau \tag{2.15a}$$

$$\dot{w}_t^{sl} = \dot{w}_t^{l} + \dot{w}_t^{+} \qquad \forall\, t \in \tau \tag{2.15b}$$

$$\dot{w}_t^{sg} \geq \dot{w}_t^{+} \qquad \forall\, t \in \tau \tag{2.15c}$$

$$\dot{w}_t^{pv} \geq \dot{w}_t^{+} \qquad \forall\, t \in \tau \tag{2.15d}$$

Constraints (2.15a) and (2.15b) enforce energy balance for the grid module on system generation and load, respectively. Constraints (2.15c) and (2.15d) are conditional constraints depending on specific requirements imposed on the hybrid system's battery charging. Constraint (2.15c) limits battery charging to only electricity produced by the hybrid system locally, i.e., the battery cannot be charged by the electric grid. Constraint (2.15d) restricts battery charging to only electricity generated by the PV system. Constraint (2.15d) is more restrictive than Constraint (2.15c); therefore, Constraint (2.15c) can be omitted if Constraint (2.15d) is imposed.

2.2.2 Operational Costs

The dispatch behavior of the the objective functions ($\mathscr{H}_1$) and ($\mathscr{H}_2$) depends on the values of the cost coefficients for each technology. For example, if the battery lifecycle cost, C^{bl} exceeds the revenue generated from a discharging operation (for the ($\mathscr{H}_1$) objective) or exceeds the cost of missing a desired load (for the ($\mathscr{H}_2$) objective), then the battery will not discharge. Similar examples can be constructed for the CSP system dispatch. As a result, the hybrid dispatch profile can be sensitive to the assumptions around cost coefficients and electricity pricing. This sensitivity is valuable as it allows the hybrid dispatch model to make decisions about charging and discharging storage assets based on the electricity price available to the system. However, if the electricity price is too low compared to the operating costs, the hybrid dispatch model will choose to not operate the system.

Table 7 presents the default values used for the cost coefficients within the hybrid dispatch model ($\mathscr{H}$). These values can be adjusted to meet other requirements or assumptions. The power cycle generation, startup, and change-in-production (ramping) costs were estimated based on Kumar et al. (2012). Generation cost of PV was estimated using the SAM default operation and maintenance costs for PV systems, which were $15/kW-yr (fixed cost by capacity) (National Renewable Energy Laboratory 2021). The battery lifecycle cost is estimated using the SAM battery model. In future work, these operating cost parameters and dispatch solution sensitivity should be further investigated and understood.

Table 7. Hybrid dispatch cost coefficient default values. †The parameter value is scaled based on sub-system capacity.

Description	Symbol	Value	Units
Generation cost for the CSP field and receiver	C^{rec}	0.5	[\$/MWh$_t$]
Fixed cost for receiver startup	C^{rsu}	1.5	[\$/MW$_t$]†
Generation cost for power cycle operation	C^{pc}	2.0	[\$/MWh$_e$]
Fixed cost for power cycle startup	C^{csu}	40.0	[\$/MW$_e$]†
Penalty for change in power cycle thermal input	$C^{\delta x}$	0.5	[\$/MW$_t$]
Generation cost of PV field	C^{pv}	1.7	[\$/MWh$_e$]
Operating cost of charging battery	C^{bc}	0.9	[\$/MWh$_e$]
Operating cost of discharging battery	C^{bd}	0.9	[\$/MWh$_e$]
Lifecycle cost for battery	C^{bl}	26.5	[\$/MWh$_{dc}$-cycle]†

2.2.3 Example Dispatch Profiles

Figures 6–9 provide examples of simulation results for four different single-technology or hybrid systems. Each simulation uses 2012 weather data for Daggett, California, and an hourly price signal taken from the Cambium 2020 database for model year 2030 (Gagnon et al. 2020). Weather data from 2012 was used to be consistent with the weather data used to generate the Cambium database. The profiles presented in Figures 6–9 illustrate days 110–115 of the simulated year, i.e., April 20–25. All CSP + TES systems are molten-salt power tower systems, and all PV systems are single-axis tracking. A time-independent grid limit of 100 MW$_e$ is imposed in each case, and the dispatch optimization model is based on the $\mathscr{H}_1$ objective, which seeks to maximize net revenue.

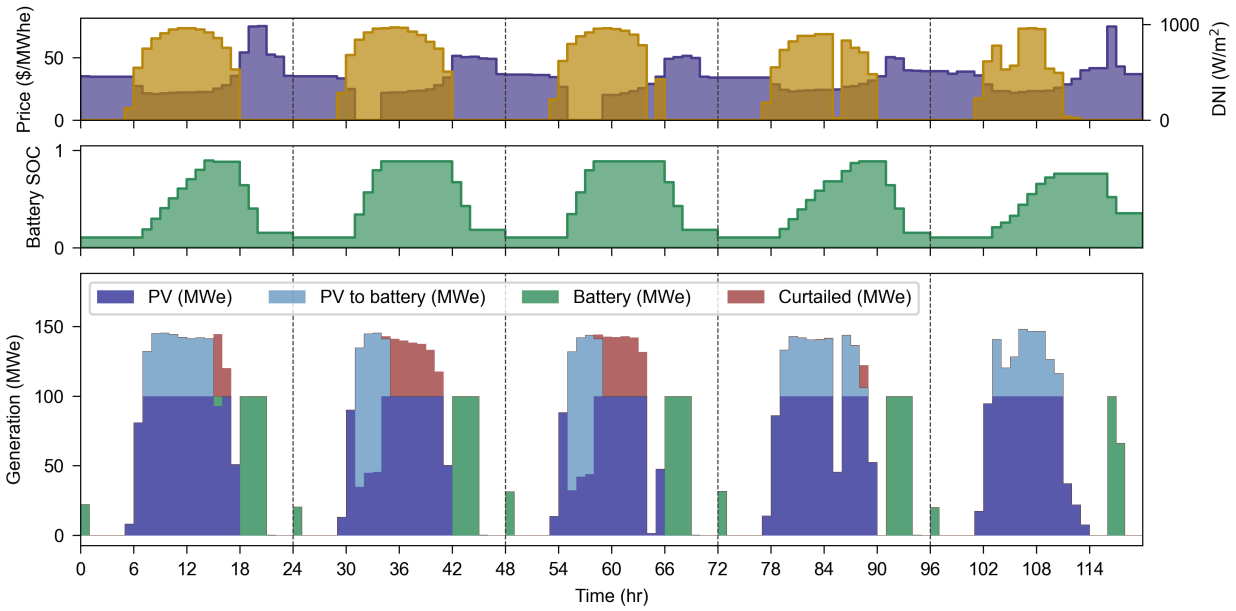

Figure 6. Example simulated dispatch profile for a PV + Battery system with a 200 MW_e (DC) PV array, DC-to-AC ratio of 1.5, 100 MW_e / 400 MWh_e battery, and a grid limit of 100 MW_e.

Figure 6 shows results from a PV + Battery case with a 200 MW_e (DC) PV array, a 1.5 DC-to-AC ratio, and a 100 MW_e battery with 4 hours of storage. Excess output from the PV array is first used to charge the battery, and is later curtailed when the battery state of charge (SOC) reaches capacity. Battery discharge occurs soon after sunset, in response to an increase in electricity price. The PV array provides electricity to the grid even during periods when the electricity price is equal to zero, despite a slight O&M cost associated with PV generation (Table 7). This is a result of the lack of feedback between the dispatch solution and performance of the PV field described in Section 2.1.1. As described in Section 2.1, the mixed-integer linear dispatch optimization model provides control signals to the more rigorous and nonlinear technology performance models that are used to simulate hourly operations. In some cases, the nonlinearity inherent in the technology performance models leads to slight discrepancies between how the dispatch optimization model expected the system to perform when determining optimal operations, and how system actually performs when simulated subject to the optimized control signals. This can lead to differences in expected versus actual stored energy or net electricity generation. These discrepancies account for the small quantity of energy dispatched from the battery at 12–1 a.m. each day in Figure 6. The battery SOC is re-initialized to the value obtained from the nonlinear performance model when the dispatch horizon rolls forward every 24 hours. A higher-than-expected end-of-day battery SOC from the technology performance models may be dispatched early in the subsequent optimization horizon such that the battery can utilize more PV electricity during that subsequent day that would otherwise need to be curtailed. Had the dispatch model known this slightly higher SOC would be available, it may have chosen to utilize it during higher-price periods on the previous day. As future work, this modeling artifact could be minimized by increasing the frequency of re-syncing the dispatch model initial conditions with the performance model.

Figure 7 illustrates the operation of a stand-alone CSP molten-salt power tower plant during the same set of days illustrated in Figure 6. Here, the gross capacity of the power cycle is equal to the grid limit (100 MW_e), the thermal storage has capacity for 15 hours of full-load design-point cycle thermal input, and the solar multiple (the ratio of the design point solar field and receiver output to the design point power cycle thermal input) is 2.5. The simulated combination of solar multiple and thermal storage capacity is not quite large enough for the power cycle to operate at full load during the entirety of each day, particularly when the solar resource is not ideal, e.g., during periods of intermittent cloudy weather or shorter winter days. The CSP power cycle remains "on" during the entirety of the five-day period in Figure 7, periodically ramping down to near minimum load to avoid emptying storage and thereby avoiding an additional power cycle startup. This preference for minimum-load operation over on/off cycling is sensitive to the reduction in cycle thermal-to-electric efficiency at low load conditions and the assumed power cycle startup and ramping cost (Table 7). Figure 7 illustrates net electricity generation, which is derived from gross

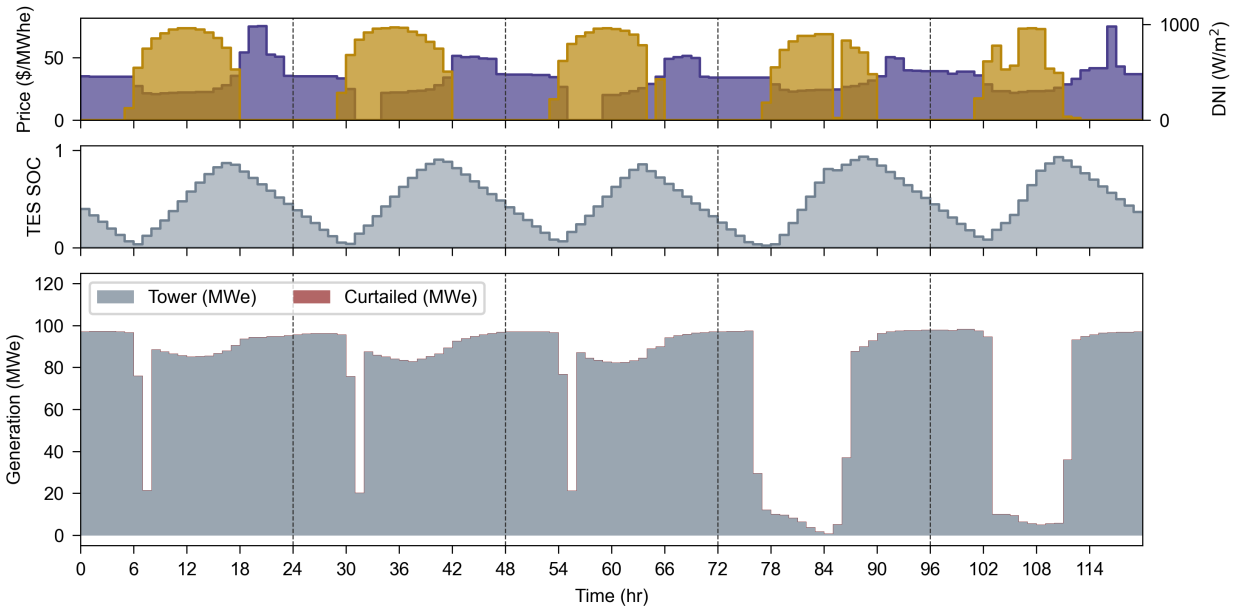

Figure 7. Example simulated dispatch profile for a CSP + TES system with a 100 MW_e (gross) power cycle, solar multiple of 2.5, 15 hours of thermal storage, and a grid limit of 100 MW_e.

electricity generation less parasitic loads associated with operating the CSP plant. The decrease in net electrical output during the solar day arises from the combination of parasitic loads associated with operating the solar field and receiver and a higher mid-day ambient temperature, which reduces the power cycle efficiency. Similarly, the near-zero net output on the latter two days in Figure 7 occurs when the power cycle operates near the minimum operational limit (based on thermal input), but the majority of the gross electrical output is used to support parasitic loads of the solar field and receiver.

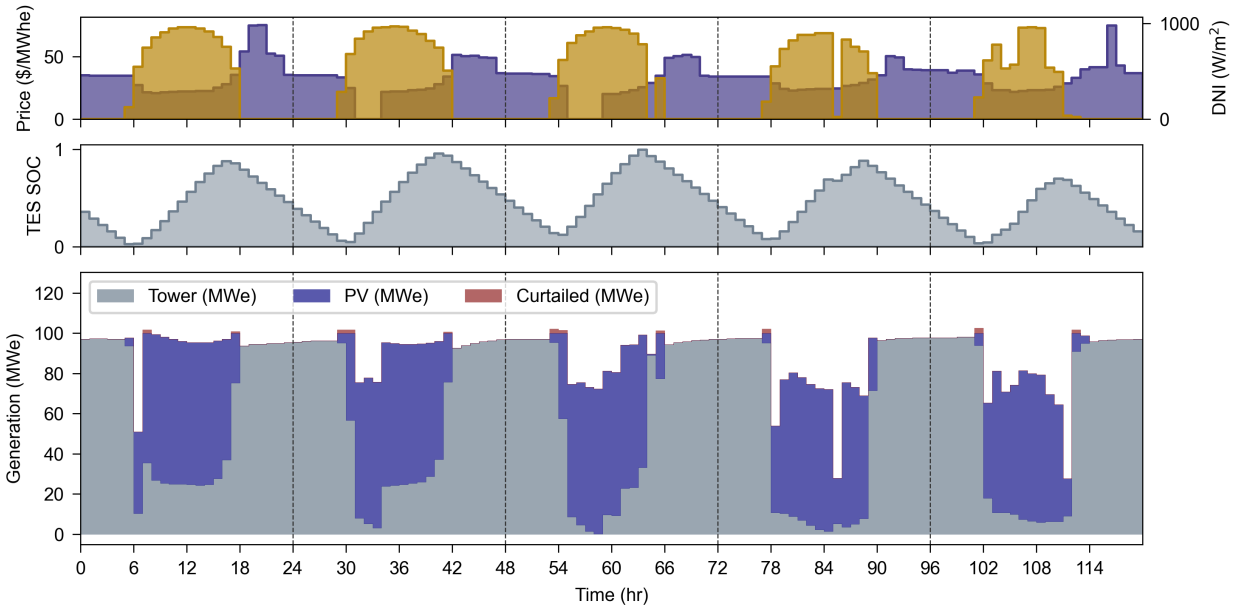

Figure 8. Example simulated dispatch profile for a CSP + TES + PV system with a 100 MW_e (gross) power cycle, solar multiple of 2.0, 15 hours of thermal storage, 100 MW_e (DC) PV array, DC-to-AC ratio of 1.5, and a grid limit of 100 MW_e.

Figure 8 provides simulated operational profiles for a hybrid CSP + TES + PV system. Here, the CSP power cycle gross capacity is 100 MW_e and the system has 15 hours of thermal storage capacity, but the solar multiple was reduced to 2.0 (from 2.5 in Figure 7) as a 100 MW_e (DC) PV array provides electricity during daylight hours. The CSP power cycle operates around the output from the PV array, ramping down to low-load conditions during daylight hours, and ramping up to near full-load conditions after the sun sets. Slight curtailment of the PV generation near the beginning and end of each simulated day can be noted in Figure 8. This occurs because the linear dispatch optimization model cannot fully capture the non-linear behavior of the CSP receiver pumping parasitic loads and the cycle thermal-to-electric efficiency as a function of both ambient temperature and load fraction. At these points in time, the dispatch optimization model sets the cycle thermal input such that combination of the full output from the PV array and the expected net power cycle electricity production exactly matches the 100 MW_e grid limit. However, the full technology performance models produced slightly more electricity from the power cycle under the early morning and late afternoon conditions, leading to the small amount of curtailment noted in Figure 8. Similar to Figure 7, the power cycle remains "on" through the full simulated five-day period in Figure 8, but produces near-zero net electrical output when operating near minimum load during mid-day time periods with large parasitic loads.

Figure 9 adds battery storage to a case similar to that illustrated in Figure 8. Here, the CSP system has the same solar multiple (2.0) and storage capacity (15 hours) as in Figure 8, but the power cycle design point gross capacity is reduced to 75 MW_e, and a 25 MW_e battery is added to the 100 MW_e (DC) PV array. As in Figure 8, the CSP power cycle operates around the output from the PV array. The addition of the battery allows output from the PV array during periods of low electricity price to be stored rather than sent to the grid, and the stored energy is discharged during the evening price peak. When the mid-day electricity price is only marginally lower than the evening peak (for example, the fourth day in Figure 9), the system does not charge the battery, opting instead to utilize the PV output during the lower-priced mid-day hours. This behavior results from trade-offs between the potential for increased gross revenue when utilizing the battery, and the assumed battery operating and lifecycle costs in the dispatch optimization model. The precise values of electricity price differentials at which the model determines battery operation to be optimal will be sensitive to these assumed operational and lifecycle costs.

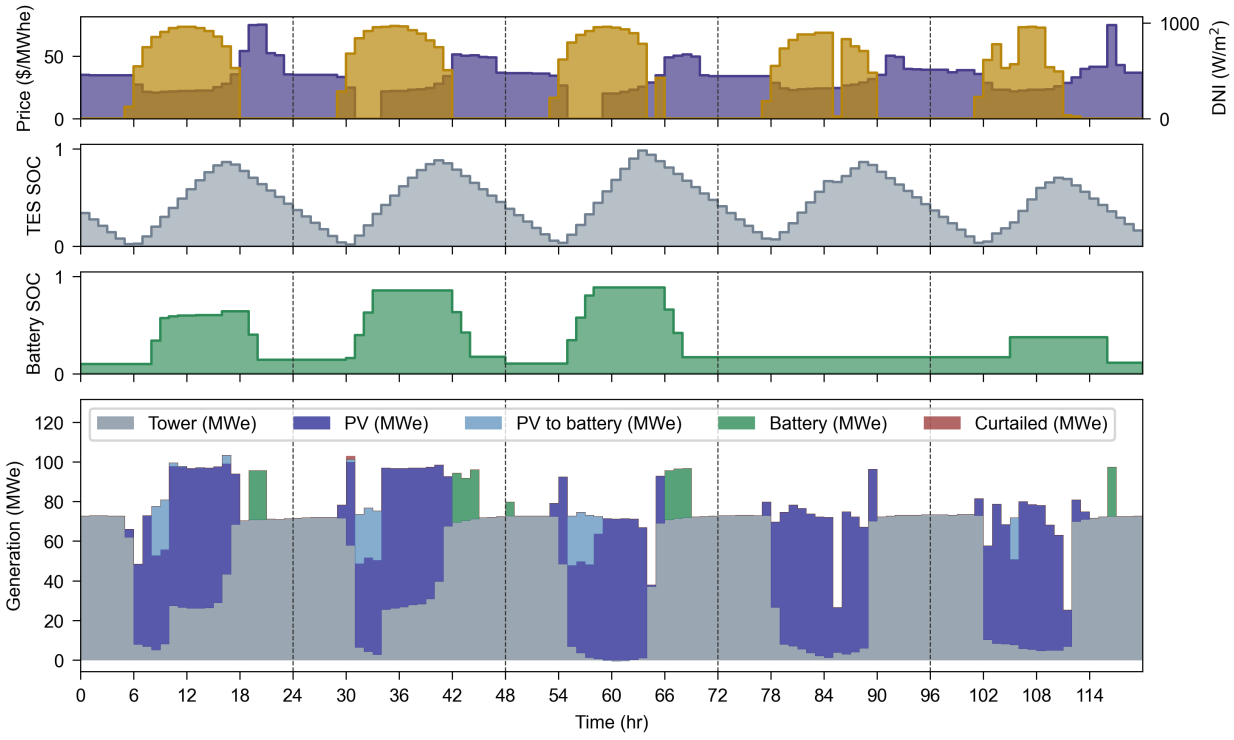

Figure 9. Example simulated dispatch profile for a CSP + TES + PV + Battery system with a 75 MW_e (gross) power cycle, solar multiple of 2.0, 15 hours of thermal storage, 100 MW_e (DC) PV array, DC-to-AC ratio of 1.5, 25 MW_e / 100 MWh_e battery, and a grid limit of 100 MW_e.

2.3 Design Analysis

Up to this point, we have focused on the methods required to simulate a single CSP-PV-battery hybrid plant. This section presents the design analysis methods integrated into HOPP. The purpose of these methods is to allow the HOPP user a way to iterate on high-level design sizing variables to better understand the specific design space. As a result of this approach, there is no "set" workflow for exploring and optimizing the hybrid system design. Instead, HOPP provides methods for reducing the required workload to implement parallel simulations, design sampling, and/or non-linear derivative-free optimization algorithms. This allows the HOPP user to create a custom design analysis workflow that addresses their specific problem.

2.3.1 Problem Driver Class

Figure 10 depicts the problem driver class, which facilitates design analysis through HOPP's design methods and interaction with the worker pool. Design analysis or iteration with HOPP poses two major challenges: (i) there is no guarantee that the design evaluation will return a successful result (i.e., without an exception) and (ii) the objective function evaluation requiring an annual simulation with dispatch optimization can be computationally expensive. The time required to run an annual simulations is in the range of 2 to 15 minutes with commercial solvers and 15 to 30 minutes with open-source solvers. However, this simulation does not require multiple CPU cores or excessive RAM for execution. This attribute of the hybrid simulation problem enables parallelization of multiple simulations if computing resources are available.

We created the problem driver class to assist with these two challenges. On initialization, the driver class either creates or reconnects to a *results cache*, which is responsible for storing the design evaluations immediately after they are returned from the worker. This functionally allows results to be stored as HOPP evaluates additional designs, which provides a method to recover results if the design analysis process fails to complete. This caching of results sequentially provides a solution to the first major challenge. Additionally, the driver will log any exception that occurs during a specific design evaluation within the cache.

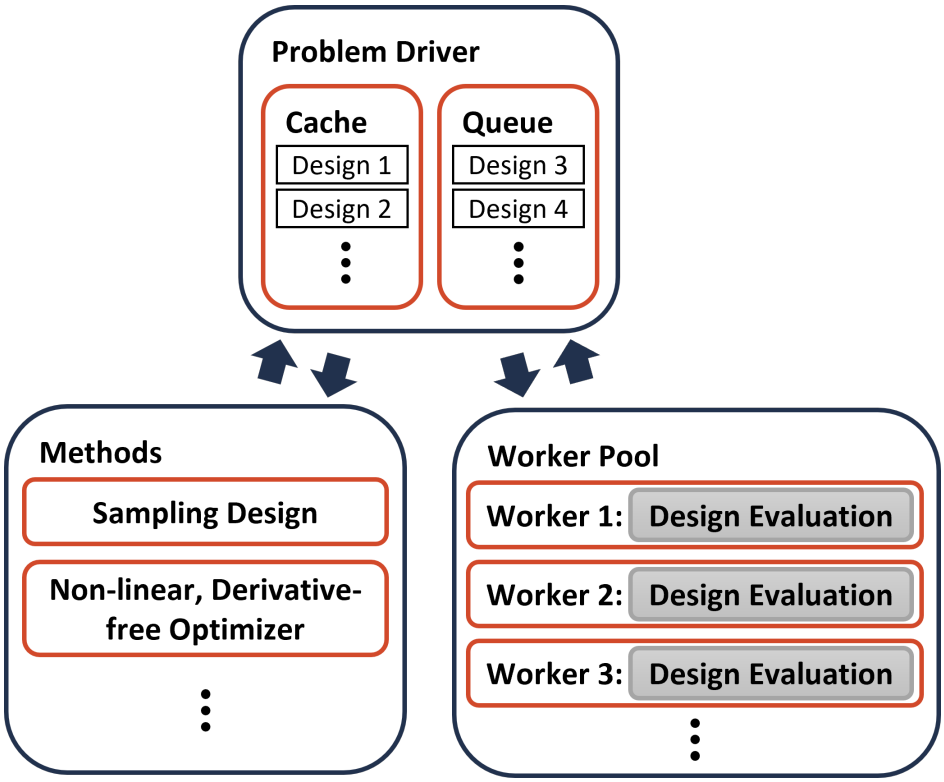

Figure 10. Simple depiction of the problem driver class facilitating design analysis through HOPP's design analysis methods and interacting with the worker pool.

To address the second challenge, the driver class checks the cache and the queue before adding a design to the queue. This removes any duplicate design evaluations. Additionally, we incorporate an optional method to reduce the

computational expense of a hybrid design evaluation via simulation of a reduced subset of days, which is discussed in Section 2.4.

2.3.2 Hybrid Sizing Problem

The *HybridSizingProblem* class was developed to house problem-specific attributes. Specifically, this class contains a *Callable* that initializes the problem's simulation and the design variables that will be iterated on through either design sampling or optimization. The simulation initializer *Callable* is a function that must be created by the user to set up the hybrid simulation with problem specific technologies within the hybrid configuration, locational weather data, electricity market pricing, and performance and financial assumptions. This *Callable* does not change as design variable iterations occur. For a given problem, the HOPP user provides a nested *dictionary* containing the problem's design variables and their associated bounds, e.g., CSP hours of TES with lower and upper bounds of 8 and 18 hours, respectively. These design variables can technically be any input parameter to SSC; however, we caution that the user should consider inter-dependencies between parameters when selecting design variables. Additionally, the problem class enables the application of fixed values to the hybrid simulation. This functionality is useful if the user wants to apply a constant value across all hybrid simulations but may want to investigate scenarios where that parameter value may be different without modifying it within the simulation *Callable*. For example, if the user wants to conduct a design study with and without capacity payments, the user can create two problem classes rather than two simulation function *Callables* that can be named accordingly. This can reduce duplicate code, which can reduce the chance of scripting errors. The process and class structure enables HOPP users the ability to set up very specific problems that they are interested in with minimum development time.

2.3.3 Design Sampling

Before executing any non-linear derivative-free optimization algorithms, it may be worth exploring the design space using sampling techniques. This approach enables preliminary investigation of the design surface being explored. Many non-linear derivative-free optimization algorithms must balance design space exploration and exploitation. Sampling is an exploration method that can be done using parallel computing resources and can provide information that may narrow the region of interest.

The problem driver provides two methods to facilitate sampling: (i) *sample()* and (ii) *parallel_sample()*. The latter should almost always be used over the former if computing resources are available to the user. These methods require a list of design candidate samples, which can be generated using any sampling method available outside of HOPP, i.e., full-factorial, uniform, Latin hypercube, etc.

2.3.4 Design Optimization

Design optimization with non-linear derivative-free optimization algorithms provides no guarantee of convergence to a local and/or global optimal solution. However, in practice, these algorithms are capable of providing valuable engineering insight and solutions. These algorithms are best paired with additional exploration of the design space, or evaluated with multiple initial starting points, to corroborate that the selected set of design variables is near optimal. Additionally, optimizer convergence and computational requirements can vary with problem dimensionality; therefore, HOPP users should try to minimize the design space dimensionality by making valid engineering assumptions for parameters that result in second-order effects.

The problem driver provides two methods to facilitate design optimization similar to sampling: (i) *optimize()* and (ii) *parallel_optimize()*. The former method should be called if the the user is only interested in using one optimizer. The latter method enables the user to use multiple optimizers in parallel to see which performs best on the problem or to compare converged solutions. These methods were written generically to work with various optimization algorithms; however, they have not been exhaustively tested for all optimizers. In this work, we have used the following *skopt* or *scikit-optimize* optimizers: *gp_minimize*, *forest_minimize*, and *gbrt_minimize*, as well as various optimizers provided by the Python package *humpday* (The scikit-optimize Contributors 2021; Cotton 2021). To the authors' knowledge, a majority of derivative-free optimizer algorithms available through Python iterate on variables using serial evaluations of the objective function. One series of algorithms that could enable parallel evaluations is evolutionary algorithms, where each generation's population could be executed in parallel; however, we have not implemented this at the time of writing this report.

2.4 Simulation Clustering

Optimization of the single-technology or hybrid system design may require consideration of numerous design variables including, for example, the relative sizing of each power generation technology, capacity of thermal energy storage (TES) and/or battery storage, solar multiple for CSP technologies, relative sizing of the PV array and inverter, minimum/maximum operational limits, etc. Each candidate set of design parameters is evaluated using optimal operational decisions via the models detailed in Section 2.2, resulting in considerable computational requirements to either rigorously optimize the system design or adequately sample designs over the full parameter space. One technique to improve the computational tractability that has been previously investigated replaces the full annual performance simulation for any given set of design parameters with a simulation involving only a limited subset of "representative" days (Martinek and Wagner 2021). The set of days to be simulated are selected via k-means or affinity propagation data clustering algorithms, based on similarity over a set of features derived from annual arrays of weather and electricity price data. For molten-salt power tower CSP systems (without PV or battery technologies), the methodology was previously found to capture annual revenue within 2.3%, 1.7%, or 1.2% for simulations involving 10, 30, or 50 three-day exemplar time blocks, respectively, and thus may be suitable for incorporation into overall design optimization problems. Here we extend the work in Martinek and Wagner (2021) to single-technology or hybrid systems involving (1) CSP + TES, (2) CSP + TES + PV, (3) PV + battery, and (4) CSP + TES + PV + battery. The incorporation of additional technologies potentially requires consideration of more features describing the weather data and/or different relative weighting of features compared to the previous application for CSP alone.

The methodology first partitions the full set of annual time-series (e.g. hourly) weather and price data into a set of overlapping four-day time blocks. The middle two days of each time block are those that, when simulated, contribute to annual generation and revenue. Each time block also includes one "previous" day that is simulated to reduce end effects for the limited time-duration horizon arising from an unknown initial storage charge state, and one "next" day that is not fully simulated but is required for dispatch optimization look-ahead. Next, each four-day time block is described by N^f representative features. These features are derived from the average of the time-series weather or price values within designated averaging periods, which are described by a specified number of divisions over either a full 24-hour period (for all quantities except those pertaining to the solar resource) or between summer solstice sunrise and sunset (for DNI and GHI). After averaging, these values are normalized based on the range of values encountered over the year, and then reduced by a feature-specific weighting factor ($0 \leq w_{feature} \leq 1$) such that different features can have differing levels of significance when identifying similarity between sets of days. The calculated set of features allows each four-day time block to be represented by a single point in N^f-dimensional space. Data clustering algorithms are then applied to this set of points to identify a set of N^c clusters comprised of similar time blocks, and to select a single exemplar time block per cluster. Finally, the time-series dispatch optimization and performance simulations are conducted for the N^c exemplar time blocks, and an approximate full annual time-series generation profile is re-created using only the simulated exemplar time blocks. Generation profiles on days that are not explicitly simulated are either set equal to the generation profile for the single exemplar time block representing the cluster to which the non-simulated day belongs (hard partitioning) or derived from a weighted average of multiple exemplar time blocks (soft partitioning). Thus, while computation of a full annual time-series generation profile traditionally requires a single continuous time-domain simulation of 365 days, this methodology reduces the number of simulated days to $3N^c$, where each of the N^c time blocks is independent in the time-domain and thereby also suitable for parallel processing. Full details are provided in Martinek and Wagner (2021) and are omitted here for brevity.

2.4.1 Weighting Factors

Selecting appropriate weighting factors and averaging periods that define the set of features describing each group of days is key to the accuracy of simulated annual generation or annual revenue. The set of possible features currently included within HOPP are: (1) DNI, (2) DNI on the previous day, (3) DNI on the next day, (4) GHI, (5) GHI on the previous day, (6) GHI on the next day, (7) electricity price, (8) electricity price on the previous day, (9) electricity price on the next day, (10) wind speed, (11) wind speed on the previous day, (12) wind speed on the next day, and (13) ambient temperature. Not all possible features should be applied to any given combination of technologies. A CSP system alone does not need to consider GHI when selecting representative days, while a PV + Battery system need not consider DNI or wind speed. Ideal weighting factors may not be known a priori, and optimal sets of weighting factors for any given simulation can be expected to depend on the nature of the weather-price scenario. For the

current incorporation into HOPP, we seek to identify sets of weighting factors for technology combinations involving CSP (CSP + TES, CSP + TES + PV, and CSP + TES + PV + Battery) that perform well over a broad range of weather-price scenarios to facilitate usage without location-specific tuning.

To this end, we selected a set of 10 weather-price scenarios and applied a combination of Latin Hypercube sampling and Bayesian optimization to identify sets of weighting factors that produced low absolute error in annual revenue over the full set of simulated scenarios. Location, weather year, and price scenarios included in the calculations are described in Table 8 and are intended to capture a variety of conditions including block schedules, real historical locational marginal price (LMP) from the California Independent System Operator (CAISO), and model-generated price signals (over a range of possible future grid scenarios) via data sets available in NREL's Cambium 2020 database for projected model years spanning 2020 to 2046 (Gagnon et al. 2020). Using multiple location/price scenarios when selecting weighting factors prevents the selected sets from being overly tuned to the specific nature of any given single scenario.

Table 8. Location, weather, and pricing scenarios used to select weighting factors for clustering. Price signals from NREL's Cambium are from the balancing area (BA) consistent with the location of the scenario.

Scenario	Location	Weather year	Price signal
S1	Rice, CA	2015	CAISO 2015 LMP
S2	Rice, CA	2012	NREL Cambium 2030, BA10
S3	Tonopah, NV	2015	CAISO 2015 LMP
S4	Tonopah, NV	2012	NREL Cambium 2030, BA12
S5	Rice, CA	2012	NREL Cambium 2046, BA10
S6	Daggett, CA	2011	SAM "Generic Summer Peak," $80/MWhe average price
S7	Albuquerque, NM	2012	NREL Cambium 2020, BA31
S8	Albuquerque, NM	2012	NREL Cambium 2030, BA31
S9	Tucson, AZ	2012	NREL Cambium 2030, BA30
S10	Tucson, AZ	2012	NREL Cambium 2046, BA30

Figure 11 illustrates fractional (absolute) error in annual revenue for various sets of weighting factors selected via Bayesian optimization for a CSP + TES case and a CSP + TES + PV + Battery case. Three different combinations of CSP solar multiple (SM) and thermal storage capacity were simulated (SM = 1 and 6 hours of storage; SM = 2 and 10 hours of storage; SM = 3 and 14 hours of storage) at each location, and points represent the root-mean-square (RMS) error over the 10 different scenarios in Table 8 and over simulations with each N^c = 20 and N^c = 30. The weighting sets in Figure 11 are sorted in order of low-to-high overall root-mean-square error over all simulated location scenarios and design configurations.

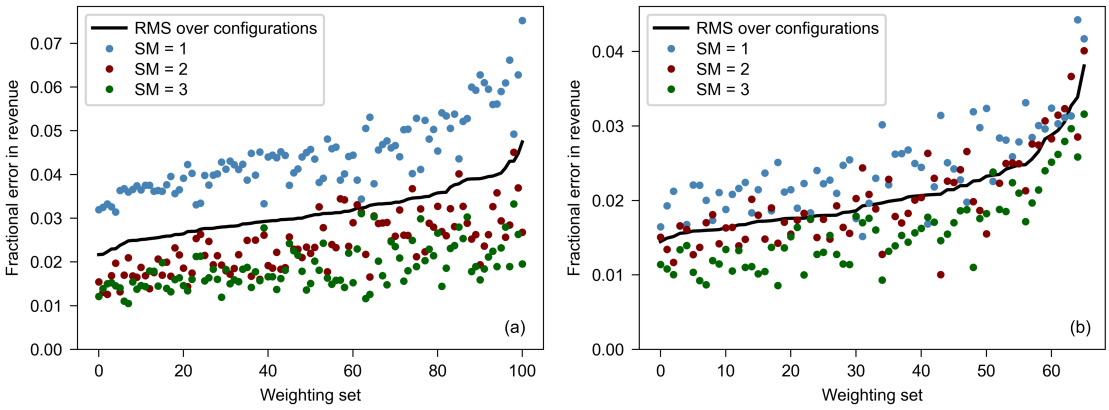

Figure 11. RMS fractional error in annual revenue over all scenarios in Table 8 with N^c = 20 and N^c = 30. Weighting sets are sorted from best-to-worst based on RMS error over all simulated design configurations for each (a) CSP + TES, (b) CSP + TES + PV + Battery.

Numerous sets of weighting factors provide, on average, <3% error in annual revenue for CSP + TES configurations, and <2% error in annual revenue for CSP + TES + PV + Battery configurations. The annual revenue from low solar multiple CSP configurations is, in general, more difficult to capture using this approach because both the quantity of available thermal energy, and the precise timing of dispatch of that energy in the simulated exemplar

day must represent all non-simulated days assigned to the same cluster. One- or two-hour shifts in the timing of electricity price peaks may not be well represented when using a small number of clusters, and can increase the error in predicted revenue.

Figure 11 provides RMS errors over all simulated scenarios; however, ideal sets of weighting factors may differ between individual scenarios. It some cases, it is possible to obtain better accuracy by tuning weighting selections to the specific scenario of interest; however, this comes with computational cost that at least partially negates the benefits of the methodology. Figure 12 provides an example of the difference in performance between locations. Figure 12 illustrates the same sets of weighting factors as in Figure 11; however, in Figure 12 these sets are sorted by low-to-high error in annual revenue for each individual weather-price scenario. The lowest errors per weather-price scenario come from a different set of weighting factors for each individual scenario and improve upon the errors illustrated in Figure 12, despite the fact that the optimization routine used to select candidate weighting sets did so on the basis of minimum error over all scnearios.

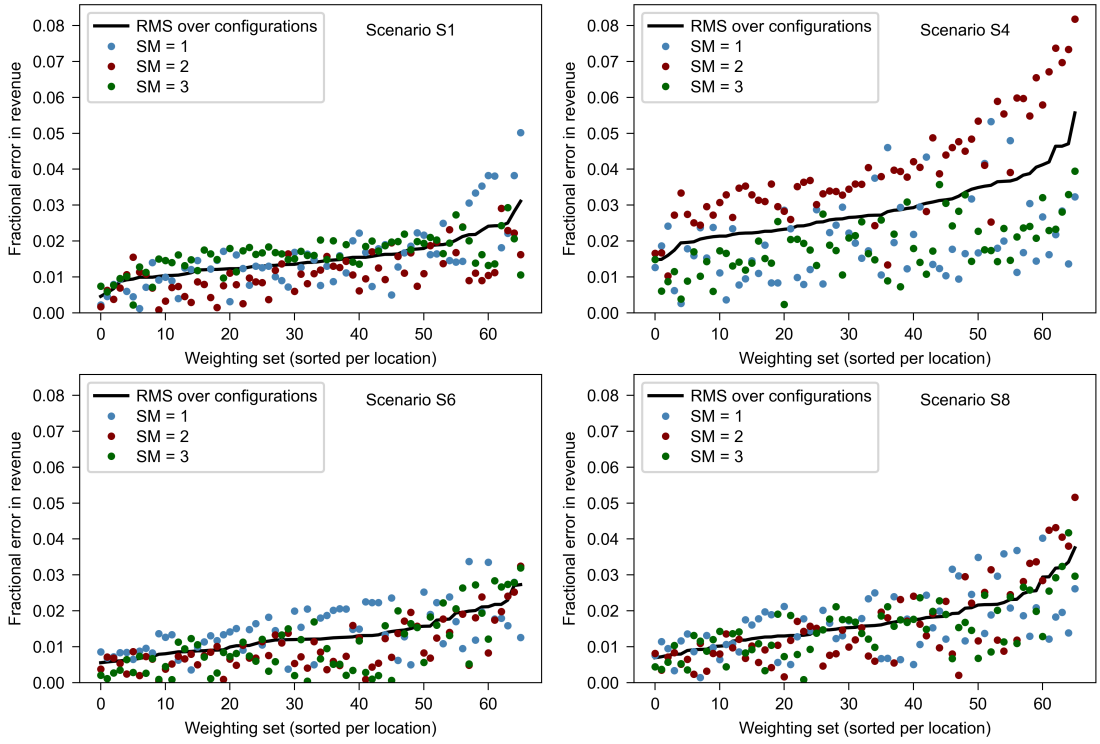

Figure 12. Fractional error in annual revenue for CSP + TES + PV + Battery cases for individual weather-price scenarios (RMS over N^c = 20, 30). Weighting sets are identical to those in Figure 11(b) but are sorted from low-to-higher error for each location.

3 Case Studies

3.1 Example Future Scenario

The following is a description of a case study of a future scenario conducted using the described modeling framework. Note that there is a high degree of uncertainty associated with the input data used in this case study, and the results can be expected to change with assumptions on both system costs and market conditions. The focus of the work described in this report was to create the modeling framework for techno-economic evaluation of CSP-PV-battery hybrid systems. We present this case study as an example of a scenario that can be evaluated using the HOPP modeling software. The absolute values of these results are sensitive to the input data. Future work could focus on developing more extensive and validated case studies for various locations, technology costs, and market conditions.

3.1.1 Input Data

For this study, we used the Solar Energy Technologies Office (SETO) 2030 cost targets for PV and CSP system costs, specifically using the "low-cost" scenario rather than the "high-performance" scenario (Solar Energy Technologies Office). As stated in the methodology section of this report (Section 2), HOPP handles PV system costs rather simplistically and only scales PV cost with installed rated DC capacity. Therefore, we aggregate the component cost breakdown to a single cost per DC capacity. This was accomplished using the default PVWatts single owner model in SAM (Version 2021.12.2), which is a 50-MW_{dc} system with 1-axis tracking. Table 9 presents the input values used in the *Installation Costs* page of PVWatts. From these inputs, the total installed cost per capacity for the PV system is $586/kWdc. We use this value within HOPP for this case study to estimate PV system cost at varying capacities.

Table 9. SAM's PVWatts installation cost parameters used to estimate HOPP's cost per DC capacity. All other inputs on the *Installation Costs* page were assumed to be zero. Assumed O&M costs are also included in this table.

Parameter	Value	Units
Module cost	0.17	[$/Wdc]
Inverter cost	0.27	[$/Wdc]
Engineering and developer overhead	0.11	[$/Wdc]
Contingency	3	[%]
Sales tax basis	100	[%]
Sale tax rate	5	[%]
O&M fixed cost by capacity	4.8	[$/kW-yr]

Table 10 presents the molten-salt power tower single-owner installation cost parameters used to approximate the SETO 2030 cost targets. The receiver and tower reference costs were estimated based on the SETO cost target of $100/$kW_t$ and the default receiver thermal rating of 670 MW_t. This case study focused on molten-salt power tower CSP technology rather than parabolic trough.

For battery system costs, we assumed $200/MW and $150/MWh, consistent with 2030 mid-cost projections presented by NREL (Cole, Frazier, and Augustine 2021). Additionally, we assumed an O&M cost equal to the PV system at $4.8/kW-yr, as well as a 10-year replacement period for the battery system.

NREL's Cambium 2020 database (Gagnon et al. 2020) was used to define the grid scenario in which in the hybrid system is presumed to operate. The tool supplies projected load and simulated hourly cost and operational data corresponding to NREL's Standard Scenarios (Cole et al. 2020), which provide projections of how the grid may evolve under various assumptions through 2050. We utilize the Cambium 2020 "Mid-Case" scenario for model year 2030. Figure 13 illustrates seasonal distributions of hourly electricity prices in the balancing area, including Southern California. Shaded bands in Figure 13 illustrate the full range and various percentiles of the data set.

The prices in Figure 13 are model-generated and subject to numerous simplifications that affect the variability and magnitude of the predicted locational marginal price (LMP). In particular, the models used to generate the data in Figure 13 consist of large balancing areas that under-represent transmission losses and transmission constraints, resulting in lower and less variable prices than would be observed in practice (Gagnon et al. 2020). Furthermore, the

Table 10. SAM molten-salt power tower single-owner installation cost parameters used to represent the SETO 2030 cost targets. All other inputs included on the *Installation Costs* page were assumed to be zero. Assumed O&M costs are also included in this table.

Parameter	Value	Units
Site improvement cost	10	[$/m^2]
Heliostat field cost	50	[$/m^2]
Tower cost fixed	1,818,300	[$]
Tower cost scaling exponent	0.0113	[-]
Receiver reference cost	62,428,300	[$]
Receiver reference area	1571	[m^2]
Receiver cost scaling exponent	0.7	[-]
Thermal energy storage cost	10	[$/kWh$_t$]
Power cycle cost	700	[$/kW$_e$]
Contingency	7	[%]
EPC and owner cost	13	[% of direct cost]
Total land cost	10,000	[$/acre]
Sales tax basis	80	[%]
Sale tax rate	5	[%]
O&M fixed cost by capacity	44	[$/kW-yr]
O&M variable cost by generation	3.5	[$/MWh]

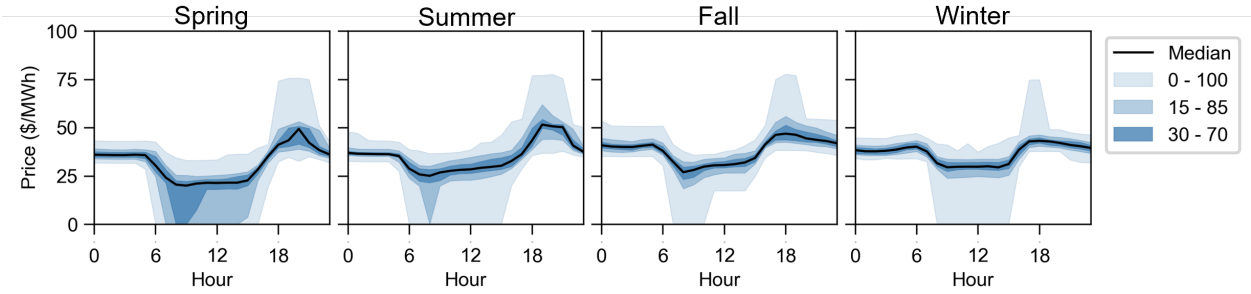

Figure 13. Daily price distributions from the Cambium 2020 mid-case scenario for model year 2030 and balancing area 10 (southern California).

models do not include a cost of carbon which, if present, would increase generation cost for coal or natural-gas fired generators.

Daggett, California, was selected as the location for the hybrid system within the balancing area represented by the prices in Figure 13, and we consider only 2012 weather data to align with the data used to generate the Cambium prices in Figure 13. To maintain day-to-day consistency between all weather, price, and net-load profiles, we simulate only through December 30, and force the underlying technology performance simulations to utilize weather data on February 29 by manually re-labeling the day/time within the 2012 weather file. Net-load (total load less variable renewable generation) for the same balancing area represented by the prices in Figure 13 was derived from the Cambium data sets for load, PV generation, and wind generation.

For this study, we assumed a capacity payment of $150/kW-yr. The capacity credit was calculated as the ratio of the sum generation during the top 100 net-load hours over the system maximum capacity (i.e., the product of nameplate capacity and 100 hours). These hours occur exclusively in the summer and early fall between the 190th and 275th days of the year, and all occur between the hours of 4 p.m. and 9 p.m. Additionally, this study assumes a 26% investment tax credit, which is consistent with the 2022 credit. However, this tax credit is planned to decrease to 10% after 2023 unless it is extended. Removing this investment tax credit or reducing it to 10% would result in higher LCOE values presented later in the results but would not change the general trends presented as all configurations are eligible for this credit.

3.1.2 Analysis Methods

For a fair comparison, we limited the "dispatchable" power rating to 100 MW_e across four CSP, PV, and battery configurations including: (i) CSP with TES, (ii) PV with battery storage, (iii) CSP with TES co-located with PV, and (iv) CSP with TES co-located with PV with battery storage. For cases (i) through (iii), the "dispatchable" power rating is defined by either the cycle generator or the battery rating. For case (iv), we defined the "dispatchable" power rating as the sum of the cycle generator and the battery rating. The reasoning behind the "dispatchable" power rating limit was to force the configuration to have the capacity to supply 100 MW_e, which enables the design analysis to focus on what surrounding assets are required to provide the "best" solution for this scenario. Additionally, we imposed a 100 MW_e transmission limit for all configurations, thereby requiring that the system effectively use storage assets to maximize revenue under this imposed limit. For example, in the CSP with TES co-located with PV configuration, the transmission limit requires CSP to collect during the solar day but dispatch electricity around PV to minimize system curtailment. This will require more energy storage than if the system was allowed to dispatch the combined CSP and PV capacity simultaneously.

The purpose of this study was to explore the design space of these systems using the modeling software described in the previous sections. To do this analysis, we first performed a Latin hypercube sampling consisting of 200 samples, then provided the sample results to three optimization algorithms as initial values, and conducted local optimization allowing each algorithm 20 iterations to improve on the solution. The algorithms used were *gp_minimize*, *forest_minimize*, and *gbrt_minimize* from the *scikit-optimize* package (The scikit-optimize Contributors 2021). The 200 samples and 20 iterations were chosen arbitrarily. Future work could focus on minimizing the number of samples and iterations required for convergence; however, these values would be problem specific.

We focused on high-level system sizing design variable decisions that have a large impact on plant performance and financial viability. Table 11 presents the design variables used in this study and their associated ranges. Cycle capacity and battery rating were varied only for the CSP with TES co-located with PV with battery storage case. In this case, the sum of the two capacity variables was required to equal the 100 MW_e "dispatchable" power rating. Therefore, the cycle capacity and battery power rating bounds are applied only when both subsystems are within the hybrid configuration; otherwise, these variables are fixed to 100 MW_e. The PV system capacity upper bound was set based on the upper bound of DC-to-AC ratio, which results in about 200 MW_e capacity, enabling generation and battery charging at 100 MW_esimultaneously.

Because of the way HOPP handles PV installed costs, DC-to-AC ratio has no impact on installed costs of PV and only impacts PV system performance. In reality, DC-to-AC ratio impacts the number and rating of inverters required for the PV system, which would impact overall system installed costs. Future work could improve the cost calculation to include this system cost scaling behavior. Lastly, the battery was restricted to charge only from the PV output and could not charge directly from the grid when electricity prices were low.

Table 11. System sizing design variables and associated ranges for each technology. †Cycle capacity and battery rating were varied only for the CSP with TES co-located with PV with battery storage case, and the sum of the two capacity variables was required to equal the 100 MWe "dispatchable" power rating.

Variable	Units	Lower bound	Upper bound
CSP with TES			
Hours of TES	[hrs]	6	16
Solar multiple	[-]	1	4
Cycle capacity†	[MW_e]	50	95
PV system			
System capacity	[MWdc]	50	325
DC-to-AC ratio	[-]	1.0	1.6
Battery system			
Energy capacity	[MWh_e]	5	1,500
Power rating†	[MW_e]	5	50

We use benefit-to-cost ratio as the design optimization objective function. HOPP defines the benefit-to-cost ratio as the ratio of the sum of annual system benefits (revenue steams) to the annualized costs of the system. Specifically,

HOPP accounts for the following benefits: (i) power purchase agreement (PPA) revenue and (ii) capacity payment revenue. All benefits and annual costs are discounted appropriately using the net present value at the start of the project. Note that the annual costs in the denominator are reduced based on investment tax credits and production credits. This metric captures the effectiveness of the system in generating revenue using time-varying prices (PPA revenue) and capacity payments, while also accounting for system costs. This objective tries to overcome the shortcomings of the more traditional project financial metrics like LCOE, which only account for the system costs and production and ignore revenue streams.

3.1.3 Results

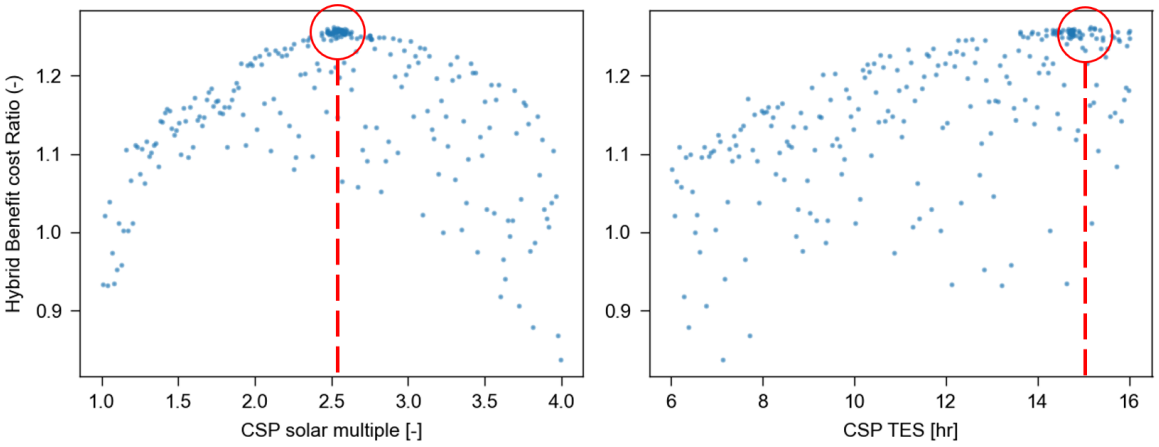

(a) CSP with TES configuration

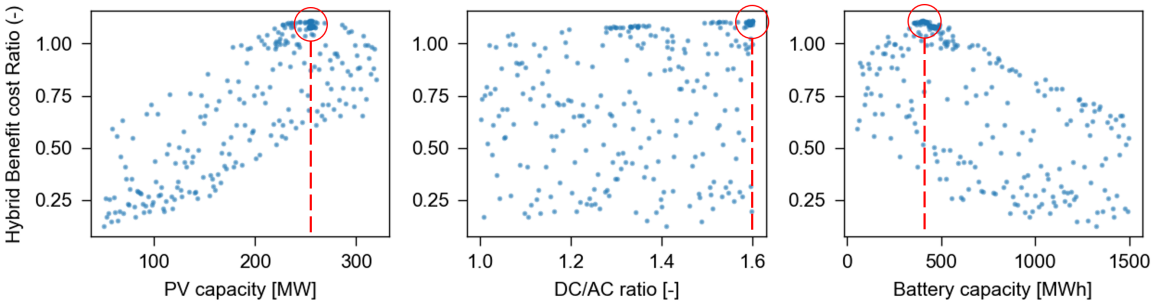

(b) PV with battery storage configuration

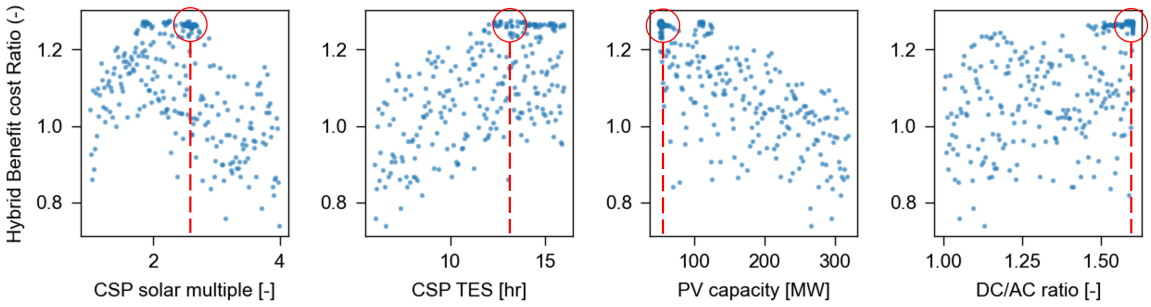

(c) CSP with TES co-located with PV configuration

Figure 14. Benefit-to-cost ratios as a function of the design variables with the "best" regions highlighted.

Figure 14 presents the hybrid benefit-to-cost ratios as a function of the design variables for the CSP with TES, PV with battery storage, and CSP with TES co-located with PV configurations. Additionally, these figures highlight the region containing the best solution found via the design sampling and optimization runs. The latter is the reason why there are more points concentrated around the region containing the best found solution.

Figure 14 provides insight into the design space under the conditions of this future scenario. From Figure 14a, the benefit-to-cost ratio increases with TES capacity, but plateaus at high TES capacity. Notice there is more sensitivity in the benefit-to-cost ratio with respect to the CSP solar multiple than with respect to the hours of TES. This sensitivity is caused by the way the CSP tower system's installed cost scales with each of these design variables. A marginal change in solar multiple will impact the heliostat field area, land area, tower height, and receiver area (all of which impact system installed cost). Note that the design variable combination for the highest benefit-to-cost ratio CSP system is not equal to the lowest LCOE configuration, which roughly occurs at a solar multiple of 3.25 and 16 hours of TES.

Figure 14b shows there is significant sensitivity in benefit-to-cost ratio with respect to PV capacity and battery energy capacity while limited sensitivity with respect to DC-to-AC ratio. This is due to DC-to-AC ratio having a minor impact on PV performance and no impact on installed costs (as stated above). Because the battery power rating is fixed to 100 MW_e, the battery energy capacity can be divided by 100 MW_e to define equivalent hours of storage. Note that the battery power rating is fixed for both charge and discharge. This limits the PV capacity that provides the battery with charging energy because overbuilding PV results in greater curtailment. Battery costs are much higher than TES costs on a cost per unit energy basis; therefore, the model determined that approximately 4 hours of battery storage is required to maximize the system's benefit-to-cost ratio.

Figure 14c presents the CSP with TES co-located with PV configuration. This configuration has approximately the same solar multiple but much lower hours of TES compared to the CSP with TES configuration. However, there appear to be two design regions with approximately the same benefit-to-cost ratio. The first region is highlighted in Figure 14c near a solar multiple of 2.5 and low PV capacity, while the second occurs with a much smaller CSP solar multiple of about 1.9 and a higher PV capacity of about 110 MWdc. This is one example of why is it important to look at the design space as a whole rather than just the single "best" point found by an optimizer algorithm.

Tables 12 and 13 present the performance and financial metrics and the design variable values corresponding to the maximum benefit-to-cost ratio found for each configuration, respectively. Table 12 indicates the worst and best values for each metric across the set of simulated technology combinations in **red** and **green** text, respectively. The maximum benefit-to-cost ratio in this case study corresponds to the CSP with TES co-located with PV configuration at 1.276, which is only a 1% increase in benefit-to-cost ratio relative to the CSP with TES configuration. This slight improvement appears to be a result of using PV generation during the solar day to cover CSP parasitic loads while simultaneously reducing the CSP solar field size (i.e., solar multiple) compared to the CSP with TES configuration, shown in Table 13. By reducing the CSP system size, the CSP-TES-PV configuration results in a slight lower capacity credit than the CSP-TES configuration. Further hybridization of CSP with PV by including an electric TES heater could potentially increase the benefit-to-cost ratio difference between the CSP-TES and CSP-TES-PV configurations, depending on the cost of an electric heater and the price electricity at which the stored PV energy could be sold. These results indicate that co-locating PV with CSP may result in a small improvement in plant financial performance under this future scenario; however, the authors believe more investigation is required to further understand the benefits of hybridizing CSP and PV technologies.

Table 12. Performance and financial metrics corresponding to the maximum benefit-to-cost ratio found for each configuration. Note the red and green text indicate the worst and best values for that metric across the set of simulated technology combinations, respectively.

Metric	CSP-TES	PV-Battery	CSP-TES-PV	CSP-TES-PV-Battery
Benefit-to-cost ratio [-]	1.263	**1.108**	**1.276**	1.225
Annual energy [GWh]	520.4	**454.0**	564.9	**643.9**
Installed cost [$-million]	336.7	**242.6**	345.2	**386.2**
LCOE (real) [$/MWh]	**42.0**	**42.0**	38.8	**38.0**
Capacity credit [%]	**89.1**	**74.3**	87.9	86.0

In this future scenario, the PV-battery configuration resulted in the worst benefit-to-cost ratio compared to the other configurations explored, shown in Table 12. The main reason for the poor benefit-to-cost ratio is the low capacity credit received by the PV-battery system, which is about 15% lower than the other configurations. Here we only consider dispatched energy, and not the combination of dispatched and stored energy, when calculating capacity

Table 13. Design variable values corresponding to the maximum benefit-to-cost ratio found for each configuration. Note the red text indicates the values that were constrained in this analysis. †Values correspond with variable bound.

Variable	CSP-TES	PV-Battery	CSP-TES-PV	CSP-TES-PV-Battery
Power cycle capacity [MW_e]	**100**	-	**100**	**95**†
Hours of TES [hr]	15.1	-	13.2	15.7
Solar multiple [-]	2.52	-	2.27	2.78
PV field DC capacity [MWdc]	-	254	53	63
DC-to-AC ratio [-]	-	1.60†	1.59	1.60†
Battery power [MW_e]	-	**100**	-	**5**†
Battery capacity [hr]	-	4	-	10 (50 MWh†)

credit. Thus, this result is due to the dispatch optimization model not having explicit knowledge of the hours contributing to the capacity payment, and the low duration of battery storage. From Figure 15, there exist designs with higher capacity credit values, approaching 100% as duration increases; however, these designs increase system costs (both installed and replacement) more than they increase the benefit of a higher capacity credit, thereby negatively impacting the benefit-to-cost ratio. Figure 15 presents an inflection point occurring around 160 MWdc where the capacity credit significantly increases with increasing PV capacity. This inflection point is where battery storage stores curtailed energy production and dispatches that energy to high-value time periods. Below this PV capacity, the PV generation does not need to be curtailed, and thus battery operational decisions are based only on the trade-off between increased revenue from time-shifting the PV electricity and battery operational costs. This results in lower battery utilization than when the battery charges from curtailed PV, and thus less likelihood of battery dispatch during the hours contributing to capacity credit. However, these conclusions can be expected to be sensitive to battery operation and lifecycle cost assumptions, as well as the battery round-trip efficiency.

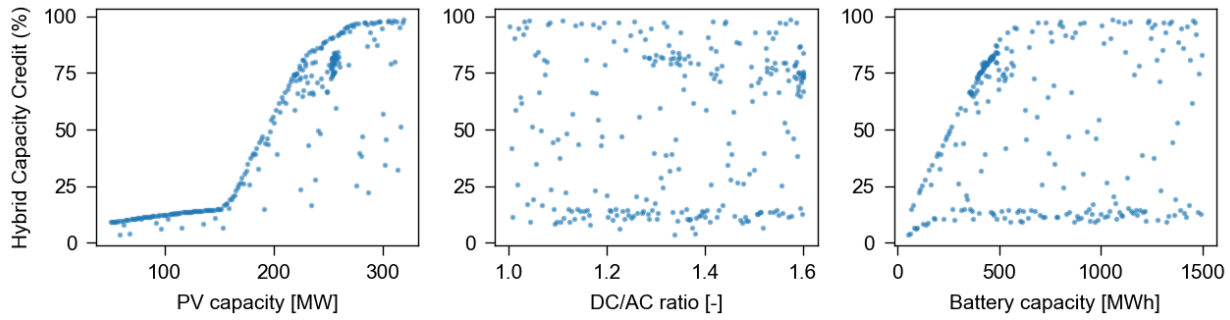

Figure 15. Capacity credit of the PV battery configuration for all the samples explored as a function of PV capacity, DC-to-AC ratio, and battery capacity.

The PV-battery and the CSP-TES configurations resulted in the same LCOE (real) value meaning that cost of electricity generation is nearly equal when compared at the same "dispatchable" power generation capacity; however, the CSP-TES configuration provides more "benefit" to the grid by providing more capacity when desired, shown in Table 12. This future scenario assumes the SETO cost targets are achieved, which would require a significant decrease in CSP and PV system costs.

From Table 13, the CSP-TES-PV-battery configuration minimizes the battery storage within the hybrid system. We expect our model to remove the battery completely, if it could, because the CSP-TES-PV configuration results in a higher benefit-to-cost ratio than the CSP-TES-PV-battery configuration, shown in Table 12. The CSP-TES-PV-battery configuration resulted in the highest annual generation, highest installed cost, and lowest LCOE (real) across all the configurations. Note that the LCOE value is reported for reference, but our analysis does not minimize LCOE; therefore, for all the configurations there exist solutions with lower LCOE values than those provided in Table 13. Additionally, our modeling analysis will favor the lower marginal energy cost of TES over batteries because the time fidelity is hourly, and thereby the model cannot reap the benefits of the more rapid response batteries can provide. A CSP-TES-PV-battery configuration would be most interesting for an island grid scenario where the system must meet 100% of the load with high reliability. In that scenario, the TES would be used for bulk energy generation while the

battery storage would be used as a buffer between PV and the TES-driven power cycle, and would handle transients between the two systems. This analysis would require sub-hourly fidelity to understand battery sizing requirements to meet a reliability metric. The HOPP framework does not preclude sub-hourly fidelity models, but the dispatch model formulation does not currently include this level of detail. However, the dispatch model could be modified to provide sub-hourly fidelity decisions in the future (Hamilton et al. 2020).

3.2 Design Space Sampling Using Representative Days

The results described in Section 3.1.3 were based on full annual simulations and did not include the techniques described in Section 2.4 to reduce computational expense. Here we evaluate if simulations using only a reduced subset of days can come to similar conclusions regarding the "best" set of sizing parameters for various technology combinations. Figures 16 and 17 illustrate the benefit-to-cost ratio for 200 sets of randomly-sampled design parameters for each PV + Battery, CSP + TES, CSP + TES + PV, and CSP + TES + PV + battery technology combinations, relative to the benefit-to-cost ratio of the best design out of the set of 200 in each case. The sets of design parameters are sorted from highest-to-lowest benefit-to-cost ratio using the results derived from full annual simulations (black points in Figures 16 and 17). Colored points illustrate the benefit-to-cost ratio for the same set of 200 designs simulated using only 10, 20, or 30 groups of representative days. All input parameters for technology costs, financial assumptions, location, weather, and electricity price are identical to those described in Section 3.1.1, and the sets of design parameters that were allowed to vary for each of the four technology combinations are analogous to those in Section 3.1.2. The benefit-to-cost ratios in Figure 17 include a $150/kW-yr capacity payment, whereas those in Figure 16 neglect capacity value.

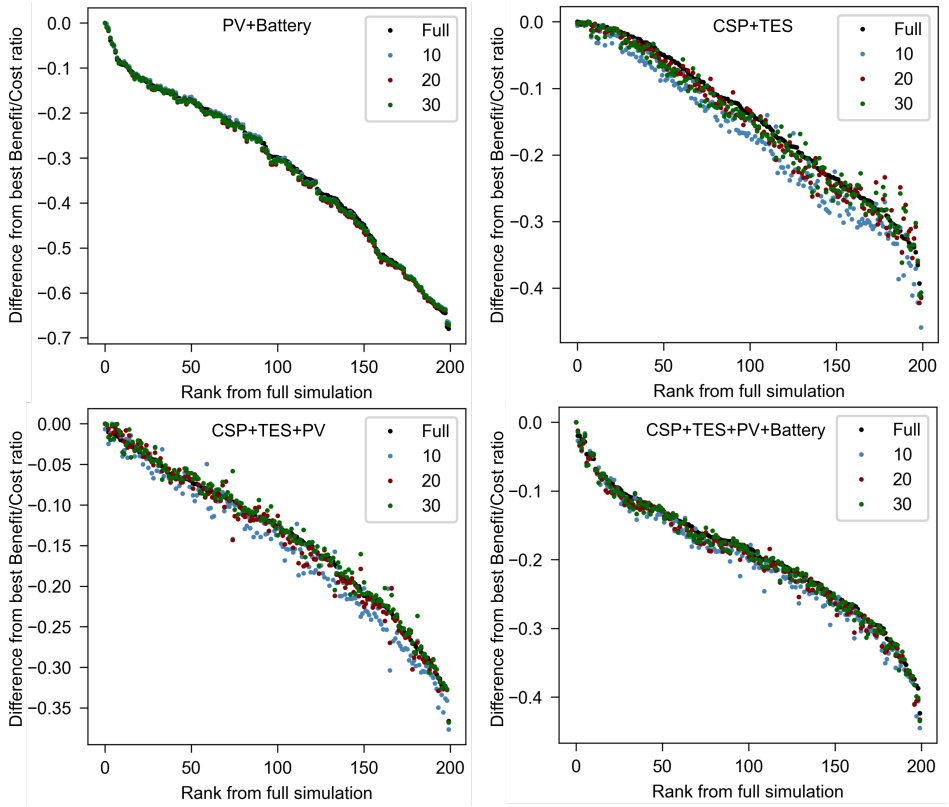

Figure 16. System benefit-to-cost ratio (relative to the best simulated design) without capacity value for 200 randomly-sampled sets of design parameters using full simulations and simulations based on 10, 20, or 30 clusters. Sets of design parameters are sorted from highest-to-lowest benefit-to-cost ratio using full simulation results.

Simulations based on subsets of representative days (colored points in Figures 16 and 17) can substantially reduce the computational burden of evaluating large sets of design parameters, but are only valuable if the reduced simulations lead to the same region of the parameter space containing the "best" design as would be identified from full simulations. Exact replication of the rank-ordering of the 200 sampled designs would be seen in Figures 16 and 17

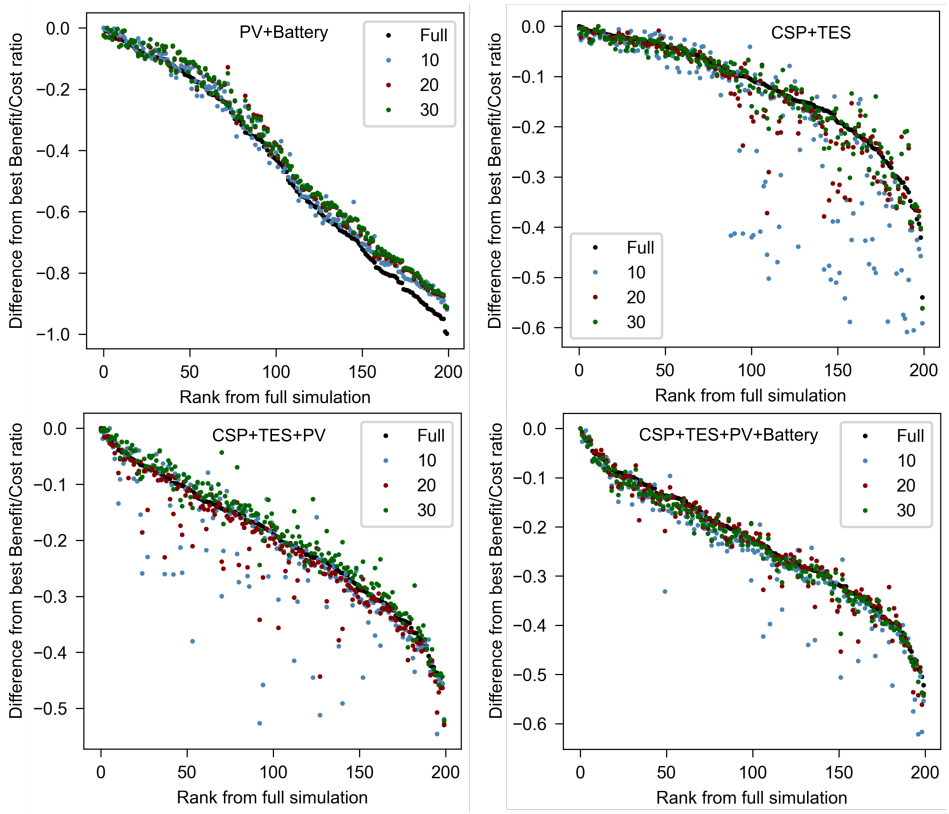

Figure 17. System benefit-to-cost ratio (relative to the best simulated design) including $150/kW-yr capacity payment for 200 randomly-sampled sets of design parameters using full simulations and simulations based on 10, 20, or 30 clusters. Sets of design parameters are sorted from highest-to-lowest benefit-to-cost ratio using full simulation results.

as a monotonically decreasing set of points. Simulations based on 10, 20, or 30 groups of representative days do not exactly replicate the relative rank ordering of every set of sampled design parameters, but do lead to a similar rank-ordering of designs over the full parameter space and similar optimal designs in Figure 16. Inclusion of capacity payments in the benefit-to-cost ratio complicates this analysis. The calculated capacity credit was derived from energy dispatched during the top 100 net-load hours occurring over the course of the year, and thus places a substantial value on a very small number of hours. The dispatch optimization algorithm does not explicitly consider the timing of these hours when selecting system-optimal operational schedules, though they are often captured indirectly via correlation between high net load and high electricity price. Furthermore, the selection of representative days did not consider these high net-load hours, and thus many of the days on which these hours occur may not have been simulated. The simulations using representative days still produced similar behavior near the optima (left-hand side of Figure 17) but can deviate substantially in other regions of the parameter space, particularly as the number of simulated days decreases. Improvements would likely be obtained via either (1) calculating capacity credit based on actual dispatch and available stored energy (as described in Section 2.1.3) or (2) modifying the methodology used to select representative days to prioritize simulation of days that contain the high-value "capacity hours."

Table 14 provides the percent difference between (1) the objective function from the full annual simulation for the best design identified from the set of 200 full annual simulations and (2) the objective function from the full annual simulation for the best design identified from the set of 200 simulations using 10, 20, or 30 clusters. Values of 0% in Table 14 imply that the full simulations and reduced simulations came to the same conclusion regarding the "best" design out of a set of 200, even though the reduced simulation may not have exactly replicated the objective function from the full simulation for that design. For this case study, the best design selected using the reduced simulations was, at worst, 2% lower in benefit-to-cost ratio (or 1.3% when considering only simulations with $N^c \geq 20$) than the best design selected using the full annual simulations.

Table 14. Difference in benefit/cost ratio for the best design identified using simulations based on 10, 20, or 30 clusters, relative to the best design identified from full simulations out of 200 randomly-sampled sets of design parameters

System	Without capacity payment			With capacity payment		
	$N^c = 10$	$N^c = 20$	$N^c = 30$	$N^c = 10$	$N^c = 20$	$N^c = 30$
PV+Battery	0%	0%	0%	0%	-0.9%	-0.9%
CSP+TES	-0.2%	-0.2%	-0.2%	-1.0%	-1.0%	-1.0%
CSP+TES+PV	-1.5%	0%	0%	-1.9%	-0.5%	-1.3%
CSP+TES+PV+Battery	0%	0%	0%	0%	0%	0%

These results illustrate that using simulations of representative days in place of full simulation results can typically reach similar general conclusions about the optimal region of the parameter space, but is not guaranteed to select the exact same "best" design within a tight margin. If more robust accuracy is required, then simulations using representative days could be used for initial screening of a wide design parameter space for a given objective function, followed by sampling or design optimization using full simulations within a more narrow window of design parameters.

Figure 18 includes additional options for objective function including nominal LCOE and net present value (NPV) in addition to benefit-to-cost ratio for a hybrid CSP+TES+PV+Battery system. Note that results in Figure 18 do not include capacity payment and that parameter sets are sorted from best to worst for each objective individually, as different objectives may lead to different optimal designs. Similar to the results in Figures 16 and 17, the sets of simulations using representative days roughly capture the relative rank-ordering of designs across multiple possible objective functions.

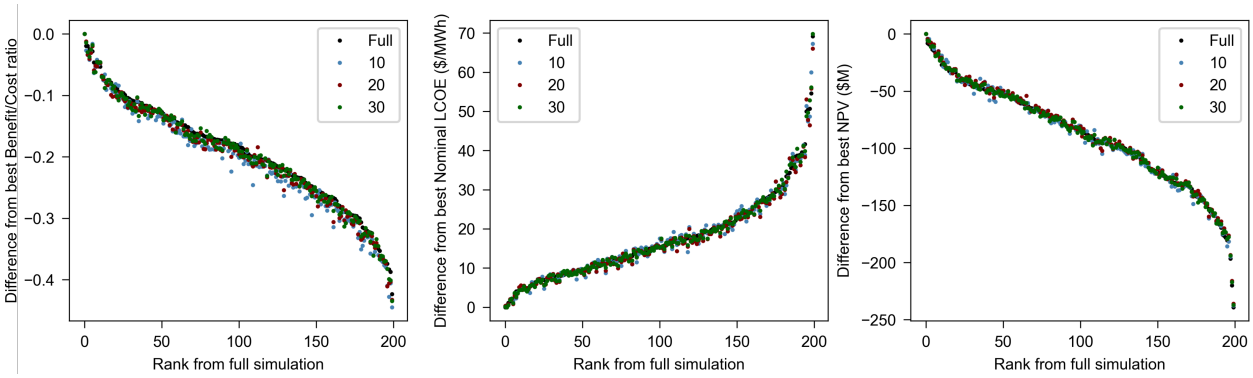

Figure 18. Objective functions (relative to the best simulated design) for 200 randomly-sampled sets of design parameters for a hybrid CSP+TES+PV+Battery system using full simulations and simulations based on 10, 20, or 30 clusters. Sets of design parameters are sorted from best to worst objective using full simulation results.

4 Summary, Conclusions, and Future Work

This work presents the methodology for integrating CSP into the Hybrid Optimization and Performance Platform (HOPP), enabling analysis of CSP systems hybridized with PV and/or electrochemical batteries (Section 2). Our contributions to this work are as follows: (i) updating HOPP's simulation class to enable CSP modeling through the HOPP software framework (Subsection 2.1), (ii) implementing a dispatch optimization model to make system control decisions that either maximize gross profit of the hybrid system or minimize load following operating cost (Subsection 2.2), (iii) developing design analysis methods and the supporting HOPP classes to facilitate various analyses (Subsection 2.3), and (iv) implementing simulation clustering to reduce computational time of annual simulations (Subsection 2.4). In addition to our methodology, the report presents a case study of a future scenario using the described modeling framework, which determines system design sizing values that maximize the benefit-to-cost ratio. We present the best designs found and their corresponding performance and financial metrics. Lastly, we conduct design space sampling using simulation clustering of representative days and draw comparisons against results derived from full annual simulations.

Integrating CSP into HOPP provides an open-source modeling platform for conducting techno-economic analysis of CSP-PV-Battery hybrids. Within this report, we exercised the developed modeling framework with future system costs (using SETO 2030 cost targets) and grid prices (using year 2030 of NREL's Cambium 2020 database). From this analysis, we determined that the CSP with TES hybridized with PV provided the best benefit-to-cost ratio compared to the other simulated technology combinations. However, this configuration only increased the benefit-to-cost ratio by about 1% compared to the CSP with TES configuration. The PV-battery system provided the lowest benefit-to-cost ratio compared to the other configurations explored because of the low capacity credit received by the system. This low capacity credit was due to the trade-off between the cost of increasing battery energy capacity and the benefit it provides to the system. Additionally, we presented the difference in benefit-to-cost ratio determined by running a full annual simulation and representative day clustering. For our case study, the best design selected using the representative day clustering was, at worst, 2% lower in benefit-to-cost ratio than the best design selected using the full annual simulations.

Our approach provides a solid methodology for modeling CSP with TES hybridized with PV as well as hybrid PV-battery systems, enabling a direct comparison of the technology configurations. This modeling framework is based on hourly time fidelity, which can provide insight about how bulk energy generation can be shifted to high-value and/or high-load hours; however, the model is unable to capture fine time-fidelity behavior that could be very valuable in balancing generation. Specifically, in a configuration that includes CSP with TES hybridized with PV and batteries, the battery could provide frequency response and a "buffer" between transitions of CSP and PV generation, which could be very valuable if the system was powering a remote load without a grid interconnect.

This report describes a modeling capability for CSP systems with TES hybridized PV and batteries. However, follow-on activities could extend this work. The following list provides ideas for future work related to the presented modeling methodology:

- Implement an electricity-to-heat pathway (e.g., electric resistance heater) for TES to further hybridize PV with CSP
- Enable controllable PV performance models allowing inverter control and/or tilt control for tracking systems
- Investigate the transition point where scaling TES system requires multiple tank pairs, and the challenges and benefits of this design
- Improve the PV system cost calculation to include the impacts of the number and rating of inverters, i.e., DC-to-AC ratio
- Perform sensitivity analysis of the dispatch operating cost parameters
- Reduce the storage inventory discrepancies between the dispatch model and the performance model

- Develop a method that minimizes the number of samples and optimization iterations required for design variable convergence
- Develop more extensive case studies for various locations, technology costs, and market conditions.

References

Cocco, D., L. Migliari, and M. Petrollese. 2016. "A hybrid CSP–CPV system for improving the dispatchability of solar power plants". *Energy Conversion and Management* 114:312–323.

Cole, W., S. Corcoran, N. Gates, T. Mai, and P. Das. 2020. *2020 Standard Scenarios Report: A U.S. Electricity Sector Outlook*. Report. National Renewable Energy Laboratory, NREL/TP-6A20-77442.

Cole, W., A. W. Frazier, and C. Augustine. 2021. *Cost Projections for Utility-Scale Battery Storage: 2021 Update*. Report. National Renewable Energy Laboratory, NREL/TP-6A20-79236.

Cotton, P. 2021. *HumpDay: A Package to Help You Choose a Python Global Optimizer*. https://www.microprediction.com/blog/humpday.

Cox, J., W. Hamilton, and A. Newman. 2022. "Optimal Sizing of a Hybrid Renewable Energy Plant". Pending, *Optimization and Engineering*.

Cox, J., W. Hamilton, A. Newman, M. Wagner, and A. Zolan. 2022. "Real-time Dispatch Optimization for Concentrating Solar Power with Thermal Energy Storage". *Optimization and Engineering*.

Denholm, P., and R. Margolis. 2018. *The Potential for Energy Storage to Provide Peaking Capacity in California under Increased Penetration of Solar Photovoltaics*. Report. National Renewable Energy Laboratory, NREL/TP-6A20-70905.

Gagnon, P., W. Frazier, E. Hale, and W. Cole. 2020. *Cambium Documentation: Version 2020*. Report. National Renewable Energy Laboratory, NREL/TP-6A20-78239.

Green, A., C. Diep, R. Dunn, and J. Dent. 2015. "High capacity factor CSP-PV hybrid systems". *Energy Procedia* 69:2049–2059.

Hamilton, W. T., M. A. Husted, A. M. Newman, R. J. Braun, and M. J. Wagner. 2020. "Dispatch optimization of concentrating solar power with utility-scale photovoltaics". *Optimization and Engineering* 21:335–369.

Hart, W. E., C. D. Laird, J.-P. Watson, D. L. Woodruff, G. A. Hackebeil, B. L. Nicholson, and J. D. Siirola. 2017. *Pyomo — Optimization Modeling in Python*. Vol. 67. Springer Optimization and Its Applications. Cham: Springer International Publishing. ISBN: 978-3-319-58819-3 978-3-319-58821-6, visited on 06/22/2021. doi:10.1007/978-3-319-58821-6. http://link.springer.com/10.1007/978-3-319-58821-6.

Hunter, C. A., M. M. Penev, E. P. Reznicek, J. Eichman, N. Rustagi, and S. F. Baldwin. 2021. "Techno-economic analysis of long-duration energy storage and flexible power generation technologies to support high-variable renewable energy grids". *Joule* 5, no. 8 (): 2077–2101. ISSN: 25424351, visited on 04/05/2022. doi:10.1016/j.joule.2021.06.018. https://linkinghub.elsevier.com/retrieve/pii/S2542435121003068.

IRENA. 2021. *Renewable Power Generation Costs in 2020*. Report. International Renewable Energy Agency, Abu Dhabi. https://www.irena.org/publications/2021/Jun/Renewable-Power-Costs-in-2020.

Jorgenson, J., P. Denholm, and M. Mehos. 2014. *Estimating the Value of Utility Scale Solar Technologies in California Under a 40% Renewable Portfolio Standard*. Report. National Renewable Energy Laboratory, NREL/TP-6A20-61685.

Kong, L.-g., X.-l. Chen, J.-h. Gong, D.-j. Fan, B.-l. Wang, and S. Li. 2022. "Optimization of the hybrid solar power plants comprising photovoltaic and concentrating solar power using the butterfly algorithm". *Energy Conversion and Management* 257 (): 115310. ISSN: 0196-8904, visited on 04/05/2022. doi:10.1016/j.enconman.2022.115310. https://www.sciencedirect.com/science/article/pii/S0196890422001066.

Kumar, N., P. Besuner, S. Lefton, D. Agan, and D. Hilleman. 2012. *Power Plant Cycling Costs*. Tech. rep. NREL/SR-5500-55433, 1046269. National Renewable Energy Lab. (NREL), Golden, CO (United States). doi:10.2172/1046269.

Liu, T., J. Yang, Z. Yang, and Y. Duan. 2022. "Techno-economic feasibility of solar power plants considering PV/CSP with electrical/thermal energy storage system". *Energy Conversion and Management* 255 (): 115308. ISSN: 0196-8904, visited on 04/05/2022. doi:10.1016/j.enconman.2022.115308. https://www.sciencedirect.com/science/article/pii/S0196890422001042.

Madaeni, S. H., R. Sioshansi, and P. Denholm. 2012. "Estimating the Capacity Value of Concentrating Solar Power Plants: A Case Study of the Southwestern United States". *IEEE Transactions on Power Systems* 27 (2):1116–1124.

Martinek, J., and M. J. Wagner. 2021. "Efficient prediction of concentrating solar power plant productivity using data clustering". *Solar Energy* 224:730–741.

Murphy, C., Y. Sun, W. Cole, G. Maclaurin, C. Turchi, and M. Mehos. 2019. *The Potential Role of Concentrating Solar Power within the Context of DOE's 2030 Solar Cost Targets*. Report. National Renewable Energy Laboratory, NREL/TP-6A20-71912. https://www.nrel.gov/docs/fy19osti/71912.pdf.

National Renewable Energy Laboratory. 2021. *System Advisor Model Version 2021.12.2*. Version SAM 2021.12.2. Golden, CO. https://sam.nrel.gov.

NREL. 2021. *FLORIS. Version 2.4*. https://github.com/NREL/floris.

– . 2022. *NREL-PySAM. Version 3.0.1*. https://github.com/NREL/pysam.

Parrado, C., A. Girard, F. Simon, and E. Fuentealba. 2016. "2050 LCOE (Levelized Cost of Energy) projection for a hybrid PV (photovoltaic)-CSP (concentrated solar power) plant in the Atacama Desert, Chile". *Energy* 94:422–430.

Scioletti, M., A. Newman, J. Goodman, A. Zolan, and S. Leyffer. 2017. "Optimal design and dispatch of a system of diesel generators, photovoltaics and batteries for remote locations". *Optimization and Engineering* 18:755–792.

Shan, R., J. Reagan, S. Castellanos, S. Kurtz, and N. Kittner. 2022. "Evaluating emerging long-duration energy storage technologies". *Renewable and Sustainable Energy Reviews* 159 (): 112240. ISSN: 1364-0321, visited on 04/05/2022. doi:10.1016/j.rser.2022.112240. https://www.sciencedirect.com/science/article/pii/S1364032122001630.

Sioshansi, R., S. H. Madaeni, and P. Denholm. 2014. "A dynamic programming approach to estimate the capacity value of energy storage". *IEEE Transactions on Power Systems* 29 (1):395–403.

Solar Energy Technologies Office. "2030 Solar Cost Targets". Visited on 03/01/2022. https://www.energy.gov/eere/solar/articles/2030-solar-cost-targets.

The scikit-optimize Contributors. 2021. *scikit-optimize Documentation Release 0.9.0*. https://github.com/NREL/scikit-optimize/scikit-optimize.

Tripp, C. E., D. Guittet, A. Barker, J. King, and B. Hamilton. 2019. *Hybrid Optimization and Performance Platform (HOPP)*. doi:10.11578/dc.20210326.1.

U.S. Department of Energy (DOE). 2021. *Hybrid Energy Systems: Opportunities for Coordinated Research*. Report. Golden, CO: National Renewable Energy Laboratory, DOE/GO-102021-5447. https://www.nrel.gov/docs/fy21osti/77503.pdf.

Wagner, M. J., and P. Gilman. 2011. *Technical Manual for the SAM Physical Trough Model*. Report. National Renewable Energy Laboratory, NREL/TP-5500-51825.

Wagner, M. J., and T. Wendelin. 2018. "SolarPILOT: A power tower solar field layout and characterization tool". *Solar Energy* 171:185–196.